Reconciling Observed and Predicted Tropical Rainforest OH Concentrations

Daun Jeong[1,a], Roger Seco[1,b], Louisa Emmons[2], Rebecca Schwantes[2,c], Yingjun Liu[3,d], Karena A. McKinney[3], Scot T. Martin[3,4], Frank N. Keutsch[3,5,6], Dasa Gu[1,e], Alex B. Guenther[1], Oscar Vega[7], Julio Tota[8], Rodrigo A. F. Souza[9], Stephen R. Springston [10], Thomas B. Watson[10], Saewung Kim[1]

[1]Department of Earth System Science, School of Physical Sciences, University of California, Irvine, California, USA.

[2]Atmospheric Chemistry Observations and Modeling Laboratory, National Center for Atmospheric Research, Boulder, Colorado, USA.

[3]John A. Paulson School of Engineering and Applied Sciences, Harvard University, Cambridge, Massachusetts, USA.

[4]Department of Earth and Planetary Sciences, Harvard University, Cambridge, Massachusetts, USA.

[5]Department of Chemistry, University of Wisconsin-Madison, Madison, Wisconsin, USA.

[6]Department of Chemistry and Chemical Biology, Harvard University, Cambridge, Massachusetts, USA.

[7]Instituto de Pesquisas Energéticas e Nucleares, Cidade Universitaria, São Paulo, Brazil.

[8]Universidade Federal do Oeste do Pará, Santarém, Brazil.

[9]Escola Superior de Tecnologia, Universidade do Estado do Amazonas, Manaus, Amazonas, Brazil.

[10]Department of Environmental and Climate Sciences, Brookhaven National Laboratory, Upton New York, USA.

[a]Now at Department of Chemistry, University of Michigan, Ann Arbor, Michigan, USA.

[b]Now at Department of Biology, University of Copenhagen, Copenhagen, Denmark.

[c]Now at Chemical Sciences Laboratory, National Oceanic and Atmospheric Administration, Boulder, Colorado, USA

[d]Now at College of Environmental Sciences and Engineering, Peking University, Beijing, China.

[e]Now at Hong Kong University of Science and Technology, Hong Kong, China

Corresponding author: Saewung Kim (saewung.kim@uci.edu)

Key Points:

- OH observations with a chemical ionization mass spectrometer during the GoAmazon2014/5 study were lower than some previous studies
- OH reactivity during GoAmazon2014/5 were substantially lower than some of the previous studies

This is the author manuscript accepted for publication and has undergone full peer review but has not been through the copyediting, typesetting, pagination and proofreading process, which may lead to differences between this version and the Version of Record. Please cite this article as doi: 10.1029/2020JD032901.

- Box model simulations of OH with five different chemical mechanisms show that observed and model-predicted OH concentrations agree to within measurement uncertainty of 40 %

Abstract

We present OH observations made in Amazonas, Brazil during the Green Ocean Amazon campaign (GoAmazon2014/5) from February to March of 2014. The average diurnal variation of OH peaked with a midday (10:00 – 15:00) average of 1.0×10^6 ($\pm 0.6 \times 10^6$) molecules cm^{-3}. This was substantially lower than previously reported in other tropical forest photochemical environments ($2 - 5 \times 10^6$ molecules cm^{-3}) while the simulated OH reactivity was lower. The observational dataset was used to constrain a box model to examine how well current photochemical reaction mechanisms can simulate observed OH. We used one near-explicit mechanism (MCM v3.3.1) and four condensed mechanisms (i.e., RACM2, MOZART-T1, CB05, CB6r2) to simulate OH. A total of 14 days of analysis shows that all five chemical mechanisms were able to explain the measured OH within instrumental uncertainty of 40 % during the campaign in the Amazonian rainforest environment. Future studies are required using more reliable NO_x and VOC measurements to further investigate discrepancies in our understanding of the radical chemistry in the tropical rainforest.

1 Introduction

Since Levy (1971) postulated the importance of hydroxyl radicals (OH) in driving the photochemistry of the troposphere, numerous modeling, laboratory, and field studies have explored its roles in determining the chemical lifetimes of reactive trace gases and producing photochemical products such as ozone (O_3) and secondary aerosol precursors such as inorganic acids (HNO_3 and H_2SO_4) and oxygenated volatile organic compounds (OVOCs). Tropospheric OH is primarily produced through O_3 photolysis and the following reaction of O (^1D) and water vapor (H_2O). The OH level is sustained by recycling processes through nitric oxide (NO) oxidation to nitrogen dioxide (NO_2) by organic peroxy (RO_2) and hydroperoxy (HO_2) radicals, generated from the oxidation of VOCs (R1 – R3). Cross ($HO_2 + RO_2$) or self-reactions ($HO_2 + HO_2$ or $RO_2 + RO_2$) between peroxy radicals compete with R2 and R3 to produce more stable compounds such as organic hydroxy peroxides. At low NO_x and high VOC environments, regeneration of OH is suppressed by these chain terminating reactions. Therefore early studies of conventional chemistry speculated OH levels are depleted in remote tropical rain forests (Jacob & Wofsy, 1988; Logan et al.,1981).

$$RH + OH + O_2 \rightarrow RO_2 + H_2O \quad \text{R1}$$

$$RO_2 + NO + O_2 \rightarrow HO_2 + RCHO + NO_2 \quad \text{R2}$$

$$HO_2 + NO \rightarrow OH + NO_2 \quad \text{R3}$$

However, numerous field observations in relatively clean forested regions have reported higher than model simulated OH concentrations, contrary to the conventional understanding of tropospheric photochemistry (Carslaw et al., 2001; Hofzumahaus et al., 2009; Lelieveld et al., 2008; Pugh et al., 2010; Ren et al., 2008; Stone et al., 2010; D. Tan et al., 2001; Thornton et al., 2002; Whalley et al., 2011). In an airborne study above the tropical forests in Suriname, Lelieveld et al. (2008) measured up to ~ 10 times higher than expected OH in the boundary layer. During the Photochemistry, Emissions, and Transport (PROPHET) campaign in a

deciduous forest in Michigan, observed OH was ~ 3 times higher than model simulations while HO_2 showed reasonable agreement (D. Tan et al., 2001). At an isoprene dominated rural region in the Pearl River Delta, China, measured OH overestimated the conventional chemistry prediction by ~ 5 times while HO_2 agreed within uncertainty (Hofzumahaus et al., 2009).

Novel OH recycling pathways were proposed to reconcile the observed OH levels (Archibald et al., 2010; Butler et al., 2008; Hofzumahaus et al., 2009; Kubistin et al., 2010; Taraborrelli et al., 2009). For example, Hofzumahaus et al. (2009) were able to reconcile the measured OH levels by forcing a hypothetical compound 'X' that is equivalent to 0.85 ppb of NO in their model simulations. Laboratory experiments (Jenkin et al., 2007, 2010) indicated that reaction between RO_2 and HO_2, which was previously thought to be a chain terminating reaction, could also produce OH. By assuming isoprene-derived peroxy radical chemistry, with an enhanced OH recycling efficiency, the model well predicted the observed OH level based on the airborne dataset from the boundary layer of a remote pristine rain forest over Surinam (Lelieveld et al., 2008). More recently, chemical reactions mechanisms, such as isoprene radical isomerization processes leading to series of reactions reproducing OH (Asatryan et al., 2010; Berndt et al., 2019; Crounse et al., 2011; Peeters & Müller, 2010; Peeters et al., 2014, 2009; Teng et al., 2017; Wolfe et al., 2012) have been proposed.

Alternative explanations for the higher than expected OH observations include positive artifacts associated with internally generated OH. Previous studies of OH measurements in high BVOC regions with the laser induced fluorescence (LIF) technique have shown that this artifact can be as much as a factor of 3 (Feiner et al., 2016; Hens et al., 2014; Mao et al., 2012; Novelli et al., 2014). Using an alternative background determining approach, the chemical removal method, by adding propane (C_3H_8) or hexafluoropropylene (C_3F_6) in the inlet to scrub OH, Mao et al. (2012) reported up to four-fold lower observed OH concentrations than the conventional background characterization method. By applying this chemical removal method, the authors were able to account for the OH levels measured at the Blodgett Forest Research Station in the California Sierra Nevada Mountains, using box model calculations embedded with the Regional Atmospheric Chemistry Mechanism (RACM2) updated with additional isoprene hydroxyperoxy radical isomerizations, suggested in previous studies (Crounse et al., 2011; Peeters et al., 2009). Novelli et al. (2014) also implemented this chemical removing method in their LIF-FAGE system in three different forested areas in Spain, Finland, and Germany. The authors found up to 30 – 80 % of OH overestimation from the recycling processes within the instrument. This study also reported that an OH intercomparison between the modified LIF and the Chemical Ionization Mass Spectrometer (CIMS), which also uses propane as a scavenger, showed good agreement between the different techniques. During the Southern Oxidant and Aerosol Study (SOAS), Feiner et al. (2016) conducted HO_x measurements with the Ground-based Tropospheric Hydrogen Oxides Sensor (GTHOS) system using LIF, at a forested region near Brent, Alabama. Compared to the method without the chemical removal, their LIF system using C_3F_6 measured ~3 times less OH during the campaign. Comparison of measured OH between CIMS and LIF, with the chemical removal background technique, during the SOAS campaign showed agreement within instrument uncertainty of 40 % (Sanchez et al., 2018). However, the extent of the instrumental interferences highly depends on the ambient conditions and details on the instrumental configurations. For instance, recent chamber and flow reactor experiments (Fuchs et al., 2016; Novelli et al., 2018; Rickly & Stevens, 2018) reported that ozonolysis of BVOCs and photooxidation of MBO by OH, which were suspected to cause internal interference within the LIF, likely generate negligible OH under atmospheric relevant conditions. Moreover, the

interference has been shown to depend on the length of the inlet and the cell pressure of the instrument (Fuchs et al., 2016; Rickly & Stevens, 2018).

Nonetheless, extensive improvements in isoprene oxidation mechanisms have been made in the past decade (Bates & Jacob, 2019; Jenkin et al., 2015; Knote et al., 2014; Saunders, Jenkin et al., 2003; Wennberg et al., 2018). Near-explicit chemical mechanisms such as the Master Chemical Mechanism (MCM) (Jenkin et al., 2015; Saunders et al., 1997, 2003) and the recently reported mechanism by Wennberg et al. (2018) include the most recent laboratory results of detailed isoprene oxidation and the subsequent reaction of hydroxy peroxy radicals (i.e., ISOPOO) with other oxidants (NO, HO_2, RO_2) and its isomerization reactions. Crounse et al. (2011) experimentally confirmed the generation of hydroperoxyenals (HPALDs) from isoprene oxidation by OH in a chamber experiment. Laboratory experiments by Wolfe et al. (2012) have confirmed that once produced, C_5-HPALDs can photolyze with a quantum yield of 1 (300-400 nm) to produce OH (yield =1). Additional OH production from this isoprene radical isomerization reaction has been further supported by Fuchs et al. (2013) through an isoprene-oxidation chamber experiment with experimental conditions similar to the field sites in the Borneo rainforest and Pearl River Delta. The conventional chemistry in the MCM v 3.2 predicted OH a factor of 2 lower than the measurements while the model embedded with the unimolecular isoprene isomerization with rate constants based on the work, presented by Crounse et al. (2011), matched well. Theses reactions have now been included in MCM v3.3.1 (Jenkin et al., 2015) with adjusted rate coefficients (Crounse et al., 2014; Peeters et al., 2015). Feiner et al. (2016) showed that box model simulations using the most recent MCM v3.3.1 were able to reproduce OH observations measured with the LIF, with the chemical background method, in an Alabama forest. However, even after considering the aforementioned observation interferences and additional isoprene oxidation schemes, there still remains uncertainties as shown in recent studies. In a chamber study by Novelli et al. (2020), model simulations with MCM v3.3.1 could not reproduce measured OH, especially in low NO_x conditions (< 0.2 ppb). A field study in a rural area near Wangdu, China, Z. Tan et al. (2017) reported higher observed OH as much as a factor of two compared to OH simulated from the RACM 2 with additional isoprene chemistry (Crounse et al., 2012; Peeters et al., 2014), when NO was below 0.9 ppb.

For practical purposes, chemical mechanisms need to be more condensed to be used in global chemical transport models so that the host model framework can run efficiently (Goliff et al., 2013). Simplifications require lumping organic compounds with comparable structure or reactivity. It is important to find a reasonable compromise so that the simplified chemical mechanism system can properly simulate ambient photochemical processes and the choice of the type of condensed photochemical mechanisms in a model should be taken cautiously depending on specific research goals (Chen et al., 2010; Dodge, 2000; Gross & Stockwell, 2003; Jimenez et al., 2003; Knote et al., 2015; Kuhn et al., 1998). For instance, Knote et al. (2015) compared gas-phase reactions of seven chemical mechanisms used in chemical transport models. The model was constrained with the same emission and meteorology parameters, and the use of different chemical mechanisms resulted in differences in simulated OH and HO_2 of up to 40 % and 25 %, respectively. The authors concluded that the discrepancies were mainly coming from differences in oxidation reactions of BVOC and nighttime chemistry.

The *status quo* motivates us to test out box model simulations of both near-explicit and condensed mechanisms and examine whether they reproduce reasonable levels of OH, especially in forested environments, where previous studies have shown significant discrepancies between the measured and modeled OH. Here, we present OH observation using a CIMS at the T3 site ~

60 km to the west of Manaus, Brazil as part of the Green Ocean Amazon (GoAmazon2014/5) research initiative (Martin et al., 2017). This is the first OH dataset measured by a CIMS in a rain forest environment. A multi-platform field campaign was conducted in 2014 in two Intensive Operating Period (IOPs) – wet (I) and dry (II) seasons. The wet season (Feb 1 – Mar 30) represents a pristine condition while the dry season (Aug15 – Oct 15) is relatively polluted from increased biomass burning. Further description of the different IOPs is described in Martin et al. (2016, 2017). We only present here the data from the first IOP. The T3 ground observation site served as a supersite to characterize trace gas and aerosol physical and chemical properties with frequent overpasses of the DOE G-1 research aircraft. The location of the T3 site was carefully selected to sample a wide spectrum of anthropogenic influences on the pristine background. Manaus, the largest city in the state of Amazonas, is ~ 60 km away and air pollution plumes were at times transported to the site during the field observation period. In order to quantitatively assess our current understanding of tropospheric photochemistry, measured OH levels are compared to observation-constrained box model simulations utilizing a suite of explicit and condensed gas-phase mechanisms.

2 Materials and Methods

2.1 Chemical Ionization Mass Spectrometer

A THS Instruments LLC Atmospheric Pressure Chemical Ionization Mass Spectrometer (AP-CIMS) was used to quantify ambient OH with an instrument configuration identical to that deployed for the 2013 Southern Oxidant and Aerosol Study (SOAS) (Sanchez et al., 2018). The mass spectrometer was housed inside an air-conditioned shed at the T3 site. The inlet sampled outside ambient air at a height of 2 m above the ground. The analytical method was developed by Tanner et al. (1997) and had mostly been used in low relative humidity environments such as the free troposphere (Mauldin et al., 1998), polar (Liao et al., 2014, 2011, 2012; Mauldin et al., 2010; Raso et al., 2017; Sjostedt et al., 2007), and non-urban regions (Kim et al., 2015; Sanchez et al., 2018). During the past few years, the AP-CIMS has been deployed in high BVOC environments and compared with ambient OH concentration reported by using LIF instrumentation (Hens et al., 2014; Sanchez et al., 2018).

As thoroughly described in Tanner et al. (1997), the AP-CIMS technique for OH quantification draws bulk air flow into the inlet (1/2" OD metal tube) with a blower. From the center of the inlet flow, a sample flow of 5 standard liters per minute (slpm) is introduced to an injector system which consists of a pair of front and rear injectors. This allows injection of a mixture of gases to convert the sampled OH into sulfuric acid (H_2SO_4) (R4 – R6). Background is characterized by adding excess pure C_3H_8 for chemical removal of OH. In an ion reaction chamber, H_2SO_4 is ionized by NO_3^- reagent ion to produce HSO_4^- (R7). NO_3^- is generated by a corona discharge ion source unit described in Kurten et al. (2011) as a zero air stream doped with HNO_3 passes over the ion source. The generated analyte ion (HSO_4^-) is introduced to a collision dissociation chamber (CDC), an octopole ion focus unit, and a quadrupole-channeltron ion detection unit, a typical configuration for mass spectrometry applications in atmospheric chemistry (Huey, 2007). A multi-point calibration was carried out as described in Sanchez et al. (2018). Briefly, OH was generated from photolysis (184.9 nm) of water in a ~ 30 slpm N_2 flow. The humidity in the calibration system was known and controlled by adjusting the fraction of N_2 flow being introduced to the water bubbler. The absolute water vapor concentration was measured by a Vaisala dew point and temperature probe (DMP 8) calibrated by a dew point

generator (LI-610). The generated photons from a UV lamp (Pen-Ray 90-004-01) was calibrated by a Hamamatsu phototube (R5764) that was calibrated by the NIST calibration facility. The calibration was conducted on a weekly basis and the precision of the calibration factor was within 10 % (1σ). The assessed limit of detection was 1 x 10^5 molecules cm^{-3} and the uncertainty was 40 % in 5 minutes for 2σ.

$$^{34}SO_2 + OH + M \rightarrow H^{34}SO_3 + M \quad \text{R4}$$

$$H^{34}SO_3 + O_2 \rightarrow {}^{34}SO_3 + HO_2 \quad \text{R5}$$

$$^{34}SO_3 + H_2O + M \rightarrow H_2{}^{34}SO_4 + M \quad \text{R6}$$

$$H_2{}^{34}SO_4 + NO_3^- \rightarrow H^{34}SO_4^- + HNO_3 \quad \text{R7}$$

2.2 Box Model Simulations

The Framework for 0-D Atmospheric Modeling (F0AM v3.2) chemical box model was used to evaluate various chemical mechanisms for simulating OH levels during GoAmazon2014/5. F0AM is a MATLAB (Mathworks®) based zero-dimensional model framework (Wolfe et al., 2016), freely available at https://github.com/AirChem/F0AM. A more recent version of the model (v. 4.0) has been released, which includes bug fixes, additional model options, and chemical mechanisms, and the model results in this study are not expected to change with the modifications made in the newer version. It has been utilized to explore the oxidation chemistry in the troposphere with observational constraints from multiple community campaigns (Feiner et al., 2016; Jeong et al., 2019; Kaiser et al., 2016; Kim et al., 2015, 2016; Wolfe et al., 2014). The box model was constrained with a comprehensive set of trace gas and meteorology measurements collected during GoAmazon2014/5. The analytical techniques and references of the observational constraints used in this study are summarized in Table S1. Alkanes and alkenes that could not be quantified by PTR-ToF-MS were adapted from Zimmerman et al. (1988). Other parameters were measured during the campaign. A total of 14 days (Feb 12-14, 16-19, Mar 5, 9, 11, 13, 15, 16, 18) were chosen during the campaign based on the availability of a complete dataset for the model simulations, excluding overcast and rainy days. Each diurnal cycle was constrained by inorganics (i.e., O_3, NO_2, CO), organics (i.e., CH_4, biogenic and anthropogenic non-methane hydrocarbons), and meteorological parameters with a time step of 5 minutes. Alkanes and alkenes from Zimmerman et al. (1988) were constrained in the model with constant mixing ratios specified in Table S1.

NO_x was not measured during the campaign due to technical difficulties along with NO_x levels often being below detection limit (LOD : 50 ppt). Therefore, NO_2 was constrained in the model by assuming to be 6 % of the observed NO_Y. Liu et al. (2016) extensively discussed the methodology to deduce NO from NO_Y using a box model and ground and airborne NO_x dataset. They concluded that NO can be reasonably estimated for their purpose of interpreting ambient isoprene oxidation product distributions at the T3 site during the GoAmazon2014/5 campaign, where the OH observation was also conducted. Isoprene reacts with OH to produce ISOPOO, which can either react with HO_2 to produce hydroxyhydroperoxides (ISOPOOH) or with NO to produce methyl vinyl ketone (MVK) and methacrolein (MACR). The relative branching depends on the level of NO. The ratio (ξ) of ISOPOOH to the sum of MVK and MACR, both measured during the campaign, was used to deduce the ratio of the corresponding production rates of each (χ). Based on the analysis by Liu et al. (2016), ξ was proportional to χ and during background

conditions (NO_Y < 1 ppb), ξ was 0.4 – 0.6 which corresponded to 0.6 – 0.9 of χ. The dependence of χ on NO was then simulated using box models embedded with MCM v3.3.1 and during background conditions, with χ ranging 0.6 – 0.9, NO was deduced to be ~ 3 % of NO_Y. The model simulated NO levels deduced by Liu et al. (2016) were well within previous NO measurements in the Amazon basin (Liu et al. (2016) and references therein). Airborne measurements during the campaign (DOI: https://doi.org/10.5439/1346559), when flying below 500 m, show a ratio of NO_2 to NO as 2.3 ± 1 (for 1σ). Therefore, in our study, NO_2 was constrained in the box model as 6 % of measured NO_Y and NO was determined in the model based on the photostationary state relationship.

For each day, we run the box model for two consecutive diurnal cycles, using the same constraints for each cycle. The first diurnal cycle is treated as a "spin-up". Sensitivity tests show that the modeled OH from the second and tenth diurnal cycles show similar results with both the slope and R^2 being 0.99 (Figure S1). Therefore, we report the second day of the diurnal cycle in this study. The hybrid method in the F0AM model was employed for photolysis rate constant calculations (J). This method calculates J values based upon assessed solar spectra from the Tropospheric Ultraviolet Visible radiation model (TUV v5.2) (Madronich & Flocke, 1998) along with cross sections and quantum yields from literature (Wolfe et al., 2016). Since the calculation was conducted with a clear sky condition, the J values were scaled to total diffuse and direct radiation between 0.4 to 4 μm, measured at the T3 site during the campaign. The clear sky solar radiation, that was used for this scaling, was derived by getting the profile of the clear sky solar radiation from the TUV model and scaling it to the maximum midday values observed during the campaign. No heterogeneous reactions were considered in the model. An additional first-order loss rate was applied to all species, with a lifetime of 6 hours following Kaiser et al. (2016). This loss term accounts for physical processes not present in the model (advection, entrainment, and deposition) and is necessary to prevent build-up of long-lived oxidation products. The sensitivity tests illustrate that the choice of the lifetime between 6 and 24 hours would not affect the OH concentration simulations (Figure S1).

Five separate mechanisms, which were readily available in the box model framework used in this study, were used for simulating OH: Master Chemical Mechanism (MCM v3.3.1), Model for Ozone and Related Chemical Tracers (MOZART-T1), Carbon Bond Mechanism (CB05), Regional Atmospheric Chemistry Mechanism (RACM2), and Carbon Bond 6 Mechanism (CB6r2). The total number of species and reactions of each mechanism and their implementation in 3-D model frameworks are summarized in Table 1. Specifics of lumping for each mechanism are presented in Table S2. All the presented box model runs were constrained with the identical set of chemical and meteorological parameters. The Box Model Extensions to Kinetic PreProcessor (BOXMOX) was used to run the MOZART-T1 mechanism since this mechanism was not included in F0AM. BOXMOX is an extension to the Kinetic PreProcessor (Knote et al., 2015) that uses a Rosenbrock solver. Comparisons between the two box models embedded with the identical MCM v3.3.1 mechanisms and observational constraints showed good agreement (Figure S2), which justify the comparisons of the model results between the two different model frameworks.

3 Results

3.1 Observation Results during GoAmazon2014/5

Figure 1 shows the 14 days of OH dataset used in this study. Bakwin et al. (1990) reported background conditions of NO_Y in the Amazon rainforest during the wet season to be below 1 ppb based on the probability distribution of data collected from the whole observation period (April to May of 1987). As shown in the variation of NO_Y in Figure 1, enhanced levels of NO_Y were frequently observed, most likely from pollution plumes from Manaus. Diurnal averages and standard deviations of the 14 days of measured isoprene, total MVK and MACR, monoterpene, toluene, benzene, and CO are shown in Figure 2. Based on the observations of VOCs, isoprene is the most dominant OH sink in this environment consisting about 56 % of midday OH reactivity (Figure S5).

The observed midday averaged OH level is significantly lower than those from the previous field campaigns in similar photochemical environments as shown in Table 2. Among the examples, GABRIEL, PROPHET, OP3, and Wangdu reported substantially higher OH than the CABINEX, BEARPEX09, SOAS, and GoAmazon2014/5. BEARPEX09 and SOAS used chemical removal method in their LIF system to determine background OH. During CABINEX and the study in Wangdu, chemical removal method was tested out and the interferences were concluded to be within the instrumental uncertainty. The campaigns presented in Table 2, regardless of geographical differences, have two similarities. First, biogenics are the dominant OH sink among the quantified trace gases. Second, NO is below 100 ppt and close to 50 ppt and so can be categorized as a low-to-moderate NO regime based on the expected fate of peroxy radicals. In the case of the Wangdu study, it was at a rural site near (< 200 km) some large cities and therefore had a higher NO_x level. For the BEARPEX 09 site, the local emissions were mostly 2-methyl-3-buten-2-ol (MBO) and monoterpenes but isoprene was transported to the site from a nearby oak woodland area in the afternoon (Mao et al., 2012). OH reactivity, which is the inverse of OH lifetime, was relatively lower in PROPHET, CABINEX, Wangdu, and GoAmazon than other campaigns in Table 2.

3.2 Comparison between Observed and Modeled OH

With the observational dataset collected during GoAmazon2014/5, box model simulations were run for five different chemical mechanisms. Figure 3 shows the model simulation results along with the OH observations on the corresponding day. In most of the days, all five chemical mechanisms (i.e., MCM v3.3.1, RACM2, CB05, CB6r2, and MOZART-T1) generally agreed well with the OH measurements within the instrumental uncertainty. Among the 14 days presented in this study, 12 days (February 12th, 13th, 14th, 16th, 17th, 18th, 19th, March 5th, 9th, 11th, 13th, and 16th) showed model estimates were within uncertainty of the OH observations for most of the day except March 18th and March 15th. For March 18th, the five model simulations underestimated the observations up to 5-fold. For March 15th, all mechanisms overestimated the measurements up to 3-fold. The agreement between the model simulations and the observations were the highest at midday with more discrepancies earlier or later in the day, which is consistent with the findings reported by Sanchez et al. (2018) for the SOAS dataset. Figure 4 shows correlation between OH observations and model results from 5 different chemical mechanisms. The red lines are linear trend lines of the correlations between modeled and observed OH. The results illustrate that the agreement is in general within the 40 % uncertainty of the measurement throughout the OH range for the model runs with MCM v3.3.1,

CB05, CB6r2, RACM2, and MOZART-T1 mechanisms. This finding is consistent with Mao et al. (2012) and Feiner et al. (2016) where they reconciled the observed OH with model simulations. During BEARPEX09, Mao et al. (2012) measured OH with the LIF using the chemical removal method at a ponderosa pine forest in Sierra Nevada. In their study, the authors were able to reconcile the observed levels of OH through box model simulations embedded with the RACM 2 mechanism with additional isoprene chemistry. An identical conclusion was presented by Feiner et al. (2016) with the SOAS dataset where they compared observations with box model runs with MCM v3.3.1. Indeed, the OH reactivity during GoAmazon2014/5 was relatively low, which could lead to a less pronounced production of unexplained OH if there were any. Rohrer et al. (2014) summarized previous field campaigns with high OH reactivity (> 10 s^{-1}) and showed that unexplained OH production persisted in low NO_x environments compared to studies in pristine environments with low OH reactivity (e.g., Holland et al. (2003)). In addition, according to Mao et al. (2012) and Novelli et al. (2017), the interference from the wave modulation method in LIF was more pronounced with increasing OH reactivity and temperature, which is indicative of higher terpene emissions. SOAS and BEARPEX were carried out in a high OH reactivity environment (Table 2) and observed up to a factor of three of interference from the wave modulation method compared to the chemical removal method. In comparison, CABINEX and Wangdu had lower OH reactivities, more similar to GoAmazon2014/5, and reported interferences within instrumental uncertainty and the model simulations still matched the observations generally well. On the other hand, it is also possible that the total OH reactivity during GoAmazon2014/5 was higher than the model simulations in this study. The model simulations only account for the constrained compounds and its oxidation products within the chemical schemes of each reaction mechanism. Any unidentified or unobserved compounds are therefore not considered in the modeled OH reactivity. However, our midday averaged total OH reactivity (~8 s^{-1}), simulated by an observationally constrained box model, corresponds to what Nolscher et al. (2015) measured near the ground (~ 7 s^{-1}) of the Amazon rainforest and inside the canopy (~10 s^{-1}) during the wet season. In our study, isoprene was the dominant sink for OH, accounting for ~ 56 % of simulated total OH reactivity in the midday (Figure S5). This is consistent to Nolscher et al. (2015) where they reported that 60 % of the total measured OH reactivity was explained by isoprene during the wet season at midday. Moreover, their study reported that missing OH reactivity at midday during the wet season was on average 5-15%, within the uncertainty (16 %) of the measurement. Therefore, we don't think the discrepancy between the modeled and measured OH reactivity would be significant in our study since the observations were carried out during the wet season. During GoAmazon2014/5 we did not see a clear trend in the extent of discrepancy between modeled and observed OH with respect to the level of isoprene (Figure S10). A follow up study in a similar environment with higher isoprene levels is required to directly measure total OH reactivity and compare them to previous studies with higher OH reactivity.

One uncertainty in the model runs originates from how NO_x is treated in the simulations. As described in the methods, NO_2 was assumed to be a fixed 6 % of observed NO_Y. However, these assumptions are based on background conditions and the ratio of NO to NO_Y could vary, which could result in substantial changes in simulated OH level if the model is sensitive to constrained NO_2. Among the OH measurement used in this study, 35 % of data points were during the background conditions of NO_Y (< 1 ppb). The diurnal variations of measured NO_Y and estimated NO_X for each case day are summarized in Figure S4. Moreover, since NO was assumed to be in photostationary state with NO_2, if there were any significant source of fresh NO

emissions near the observation site, for example from soils (Alaghmand et al., 2011), this could lead to uncertainties in modeled OH. NO emission from Manaus, however, is expected to reach photostationary state by the time it reaches the observation site, which is several hours downwind (Liu et al., 2016). In order to examine the potential uncertainties in the model caused by the NO_x estimation method applied in this study, sensitivity tests were carried out by constraining different NO_2 levels in the model embedded with MCM v 3.3.1. As in Figure 5 (a), doubling the constrained NO_2 resulted in ~40% higher OH at midday. Although this is within the instrumental uncertainty, it illustrates that the simulated OH is sensitive to how NO_2 is constrained in the model runs. Quadrupling the constrained NO_2 resulted in a factor of ~2.5 of midday OH. For example, on March 14th, which was not included in the 14 selected days, midday NO_Y ranged between 1 – 3 ppb. OH model simulations constrained with observation from Mach 14th, resulted in an overestimation of ~3-5 fold compared to observations. This is above the background NO_Y levels and the airmasses were likely affected by pollution from Manaus, as shown in the back trajectories in Liu et al. (2016). Therefore, deriving NO as 3 % of measured NO_Y might not be applicable in some observation periods selected for the model simulations in Figure 3. However, we were not able to identify a clear dependence of the discrepancy between measured and modeled OH with varying NO_x levels as presented in later parts of the discussion (Figure 7b). We acknowledge that the lack of NO and NO_2 observations during GoAmazon2014/5 is a critical limitation in carrying out a more detailed analysis and future studies with reliable NO_x observations are imperative. It should also be noted that the small alkane and alkene concentrations taken from Zimmerman et al. (1988) could be a source of uncertainty. However, sensitivity runs in Figure 5 (b), by doubling or halving the alkanes and alkene input concentrations rarely make a difference in the simulated OH, as isoprene is the most significant chemical sink of OH (Figure S5). Another feature shown in about half of the simulated days (i.e., February 12th, 13th, 16th, 19th, March 9th, and 15th) is the early morning peak of OH in the model results that occurred around 8:00 – 9:00 local standard time (Figure 6). These corresponded to a sudden peak in observed NO_Y levels, which could be from entrainment of the residual layer or influence of plume originating from Manaus. The NO_x estimation method used in our model runs, which assumes a background condition of NO_Y, could be invalid at these times.

Figure 7 illustrates the relationship between modeled and observed OH for the selected 14 days as a function of other parameters such as JO^1D, NO_2, isoprene, and O_3. Each line with markers is the binned median values of OH from observations (dashed line) and model runs (solid line) of 5 different chemical mechanisms with respect to each parameter. In order to avoid bias near the detection limit, OH observations below the instrumental detection limit were included in the analysis when deriving binned median values in Figure 7. The 5 min averaged observation data is also presented for comparison. The results show that the binned median of modeled OH from all 5 chemical mechanisms show reasonable agreement within the observation uncertainties throughout the whole range of photolysis (Figure 7a), which is consistent to what Feiner et al. (2016) reported during the SOAS campaign. According to Liu et al. (2018), noontime OH concentrations during GoAmazon2014/5 showed a positive correlation to noontime NO_Y for IOP I (wet season) and II (dry season) periods. In our study, modeled and observed OH levels, measured throughout the 14 days, increased up until 0.2 ppb of model input NO_2, which is equivalent to ~ 3 ppb of measured NO_Y (Figure S6). Since solar radiation has a strong effect on OH (Figure 7a), correlation between input NO_2 and OH was color coded with JO^1D (Figure 7b). Midday JO^1D, calculated with the F0AM model, ranged between $1 – 5 \times 10^{-5}$ s^-

^{1} (Figure S9). In background conditions (NO_Y < 1 ppb), about 35 % of the observed OH (189 points among 539 points of 5 min averaged data) was when JO^1D was above 2×10^{-5} s^{-1}. Therefore, the lower levels of OH in background conditions were not just driven by weaker solar radiation. For other parameters, the median of the model results showed agreement within uncertainty below 5 ppb of isoprene (Figure 7d) and 35 ppb of O_3 (Figure 7c), where they started to diverge. Because median values from when the divergence occurred are based on fewer data points than other bins, which showed good agreement, the bias may not be statistically relevant. However, one should note that as shown in the sensitivity tests illustrated in Figure 5, the model is sensitive to levels of NO_x and the NO_x levels estimated from relatively polluted air masses with high levels of NO_Y are more uncertain compared to that from background air masses with low levels of NO_Y. According to the chamber study by Novelli et al. (2020), modeled OH with MCM v3.3.1 still underestimated the measured OH in NO conditions below 0.2 ppb. During GoAmazon2014/5 both MCM v3.3.1 and condensed mechanisms were able to simulate OH within the instrumental uncertainties of measured OH in background conditions (i.e., NO_2 < 60 ppt) as shown in Figure 7b. As model constrained NO_2 was derived from measured NO_Y, assuming background conditions, the 35 % of the OH data points which were collected during background would have less uncertainty in the model simulations than above background conditions.

3.3 Comparison of Chemical Mechanisms

Figure 8 (a) shows comparison of steady state model simulation of midday (11:00 – 13:00) OH from MCM v3.3.1 and other mechanism (CB05, CB6r2, RACM2). Based on the linear correlation, modeled OH from the three condensed mechanisms were 6 – 15 % lower than MCM v3.3.1. Since the OH reactivity, which is inverse of the lifetime of OH, is similar between mechanisms (Figure 8b), the discrepancies in the steady state modeled OH should result from differences in OH production rate. Model simulations of midday HO_2 levels are compared between MCM v3.3.1 and other mechanisms in Figure 8 (c). RACM2 resulted in about 25 % less HO_2 than other mechanisms. This is consistent with what Wolfe et al. (2016) presented and is due to lower HO_2 production rates. RACM2 has a factor of two lower reaction coefficient for ISOPOO + HO_2 than MCM v3.3.1 (Wolfe et al., 2016) but this did not compensate the difference. Other mechanisms simulated HO_2 levels similar to MCM v3.3.1 and show that the radical chemistry is comparable between these mechanisms embedded with the observations during the GoAmazon2014/5. Modeled NO from RACM2 was slightly higher (< 7 %, Figure S7a) than MCM v3.3.1, which could be due to slower loss rates from NO + HO_2. This resulted in ~25 % less OH production rate from NO + HO_2 in RACM2 compared to other mechanisms (Figure 8d). OH production rate from O_3 photolysis was 20 % higher in RACM2 and 11 % higher in CB05 compared to MCM v3.3.1 and CB6r2. Since O_3 concentrations and photolysis rate constants (J_{O1D}) were constrained identical in all the chemical mechanisms, production rate of O^1D was the same in all four mechanisms (Figure S7b). However, O^1D loss rates from quenching reaction to O^3P were not identical due to differences in reaction coefficients, which were up to 11 % (Figure S7b). Moreover, the reaction constant of O^1D reaction with H_2O to produce two OH was 3 % higher in RACM2 than in MCM v3.3.1. Overall, these discrepancies in the reaction constants contributed up to 20 % higher OH production rate from RACM2 from $O^1D + H_2O$ compared to MCM v3.3.1 and CB6r2. Nonetheless, OH production rate in the 'others' category in MCM v3.3.1 was up to a factor of five higher than other mechanisms (Figure

8d), which compensated for the slower rates in the inorganic reactions and resulted in the highest total OH production rate. This is most possibly due to the additional isoprene reactions in the MCM v3.3.1. (Jenkin et al., 2015) which has been updated with the recent theoretical and laboratory studies (Berndt et al., 2019; Crounse et al., 2011; Peeters et al., 2014; Teng et al., 2017). This isoprene scheme has not been updated in the condensed chemical mechanisms used in our study. For comparison, OH simulations were carried out with the MCM v3.2 with model constraints identical to the MCM v3.3.1. simulations. The MCM v3.2 does not include the recent isoprene isomerization reactions and showed ~20 % less midday (11:00 – 13:00) OH than MCM v3.3.1. (Figure S8). In conclusion, the five different chemical mechanisms mostly accounted for observed OH levels during the first IOP of the GoAmazon2014/5 campaign. However, there were systematic differences between the chemical mechanisms in treating fundamental radical photochemistry in addition to differences in the isoprene isomerization reactions confirmed in recent laboratory and chamber studies, which is worth noting on evaluating regional and global photochemistry.

4 Conclusions

In this study, we reported OH observations measured with a CIMS in a rainforest during the GoAmazon2014/5. The OH levels observed were similar to previous field observations that used the LIF technique with the chemical removal method. Agreement within the instrumental uncertainty was found between measured OH and box model simulations embedded with near-explicit and 4 other condensed mechanisms used in chemical transport models. This contrasts with previous studies that reported higher than expected OH levels in forested regions, but consistent with recent results by Mao et al. (2012) and Feiner et al. (2016), where they measured OH with the modified LIF technique during BEARPEX09 and SOAS campaigns. However, the OH reactivity during GoAmazon2014/5 were substantially lower than some of the previous studies that reported significant discrepancy between modeled and measured OH. It is possible that additional unknown OH from understudied isoprene mechanisms could lead to a higher discrepancy in higher OH reactivity conditions. Moreover, BVOCs that are not measured or not identified could contribute to higher OH reactivity. Future studies at the site that encompasses a wider range of BVOC emissions and measurements of total OH reactivity would help further investigation.

Additionally, uncertainties in model simulations remain for example in model constraints and rate coefficients. NO_x observation data set during the campaign was not available due to logistical difficulties and detection limit of the instrument. Therefore, it was estimated from measured NO_Y in the model assuming background conditions. Modeled OH was sensitive to constrained NO_x levels, which highlights the importance of development of NO_x measurement techniques that can be implemented in low NO_x environments to more accurately simulate OH. The model simulations presented in our study showed agreement within instrumental uncertainty of measured OH in the environmental conditions observed during the campaign, which encompasses both background (35 %) and polluted NO_Y conditions. However, we acknowledge that the lack of NO_x measurements is a critical limitation of our analysis. Different chemical mechanisms showed distinct OH production rates from OH recycling (HO_2 + NO) and primary production (H_2O + O (^1D)), which could also be a source of uncertainty. MCM v3.3.1 showed higher levels of modeled OH compared to condensed mechanisms that do not include recent laboratory findings of isoprene isomerization reactions. Overall, while uncertainty remains, the observation and model results show good agreement within the instrumental uncertainty of 40 %

in the photochemical environment during the GoAmazon2014/5 study. Future field studies in a wider range of OH reactivity conditions, for example during different seasons, with reliable NO_x measurements will further enhance our understandings and better clarify the uncertainties presented in our study.

Acknowledgments

Institutional support was provided by the Central Office of the Large Scale Biosphere Atmosphere Experiment in Amazonia (LBA), the National Institute of Amazonian Research (INPA), and Amazonas State University (UEA). We acknowledge the Atmospheric Radiation Measurement (ARM) Climate Research Facility, a user facility of the United States Department of Energy, Office of Science, sponsored by the Office of Biological and Environmental Research, and support from the Atmospheric System Research (ASR) program of that office. Funding was obtained from the United State Department of Energy (DOE, DESC00011122), the Amazonas State Research Foundation (FAPEAM), the Sao Paulo Research Foundation (FAPESP), the Brazilian Scientific Mobility Program (CsF/CAPES), and the United States National Science Foundation (NSF). The research was conducted under Scientific License 001030/2012-4 of the Brazilian National Council for Scientific and Technological Development (CNPq). This material is based upon work supported by the National Center for Atmospheric Research, which is a major facility sponsored by the NSF under Cooperative Agreement No. 1852977. The AP-CIMS deployed for this field campaign was loaned by National Center for Atmospheric Research (NCAR) in Boulder, Colorado, USA. GoAmazon2014/5 data used in this study are available at www.arm.gov/campaigns/amf2014goamazon. The authors would like to thank Dr. Glenn M. Wolfe at NASA GSFC for the discussions on the manuscript and model simulations and Dr. Camille Mouchel-Vallon and Dr. Duseong Jo at NCAR ACOM for help on the NCAR box model BOXMOX.

Figures and Tables

Figure 1. Temporal variation of OH, isoprene, NO_Y, O_3, and solar radiation during GoAmazon2014/5. The frequency of the data is 5 min for OH, isoprene, and O_3 and 30 min for NO_Y and solar radiation. Only the 14 days chosen for this study are presented for OH.

Figure 2. Diurnal variation of measured and estimated trace gases averaged over the 14 days used in this study. Shaded areas are standard deviations of the averages. NO_2 was estimated from measured NO_Y and NO was simulated from box model simulations with MCM v3.3.1.

Figure 3. Comparison of measured and modeled OH during the GoAmazon2014/5 campaign. The box model simulations of OH were embedded with 5 different chemical mechanisms. The black line is the 5 minute averaged OH observation results and grey shades are 40 % instrumental uncertainty of the CIMS measurement. The frequency of the model simulations (markers) is 5 minutes.

Figure 4. Scatterplot of observed and simulated OH of 5 different chemical mechanisms. The blue dashed line is a 1 : 1 line with a 40 % instrumental uncertainty in shades. Each grey marker is a 5 minute data point and the red lines are the orthogonal distance regression fit between

observed and modeled OH. 5 minute averaged observation results below detection limit were included in the analysis.

Figure 5. Sensitivity of modeled OH to varying levels of (a) NO_2 and (b) VOC (i.e., alkanes and alkenes), simulated with F0AM v3.2 box model embedded with MCM v3.3.1 mechanism. 5 minute averaged OH observation data (grey marker in (a)) below detection limit is included. Only the data above detection limit is used for the averaged diurnal variation of measured and modeled OH.

Figure 6. Comparison of observed and modeled OH from MCM v3.3.1 box model, shown with measured NO_Y and modeled NO. The figure shows diurnal variations averaged over the selected days (i.e., February 12th, 13th, 16th, 19th, March 9th, and 15th), which showed enhanced modeled OH peak in the early morning. The grey shade is the standard deviation of the 6 days of OH measurements.

Figure 7. Observed and modeled OH with respect to (a) O_3 photolysis rate constant (JO^1D), (b) model input NO_2, (c) O_3, and (d) isoprene. Lines with markers are binned medians of observed and modeled OH. Grey square markers are 5 min averaged OH observation data above the detection limit for (a), (c), and (d). Figure 7b shows results of correlation between OH observations and input NO_2 below 100 ppt. Grey square markers in (b) includes data below LOD and color coded with calculated JO^1D. (Results above 100 ppt of input NO_2 are shown in Figure S6)

Figure 8. Correlation plots between MCM v3.3.1 and other mechanisms of midday (11:00 – 13:00) (a) modeled OH, (b) modeled total OH reactivity, and (c) modeled HO_2. (d) OH production and loss rates from model runs embedded with different mechanisms. The rates are averaged over midday and standard deviation of the midday averaged rates of the 14 selected days are shown.

Table 1. Chemical mechanisms used in box model simulation of OH.

Mechanism	Number of Species / Reactions	3D model	Reference
MCM v3.3.1	[a]5832 / 17224		Jenkin et al. (2015)
MOZART-T1	159 / 328	[b]CAM-Chem, WRF-Chem	[c]Knote et al. (2015)
RACM2	124 / 363	e.g, [e]CMAQ, [f]WRF-Chem	Goliff et al. (2013)
CB05	53 /156	e.g, CMAQ, WRF-Chem	Yarwood et al. (2005)
CB6r2	77 / 363	[g]CAMx	Ruiz and Yarwood (2013)

[a] Full mechanism. For the subset used in this study, 5254 reactions and 1694 species
[b] Community Atmosphere Model with Chemistry (CAM-chem), which is part of the NCAR Community Earth System Model (CESM)
[c] A preliminary version of the MOZART-T1 as published in Knote et al. (2014)
[e] Community Multiscale Air Quality system (CMAQ)
[f] Weather Research and Forecasting Model with Chemistry (WRF-Chem)
[g] Comprehensive Air quality Model with extensions (CAMx)

Table 2. Summary of OH and other trace gas measurements from various field campaigns conducted in high isoprene and low-moderate NO environments. The averaged dataset (or median if applicable) from GABRIEL, PROPHET, OP3, and BEARPEX09 are taken from Rohrer et al. (2014) . Values from the CABINEX campaign and the study at Wangdu were estimated from Griffith et al. (2013) and Z. Tan et al. (2017), respectively.

	[a]GABRIEL (Oct. 2005)	[b]PROPHET (Aug. 1998)	[c]OP3 (Apr-May 2008)	[d]CABINEX (Jul–Aug 2009)	[e]Wangdu (Jun–Jul 2014)	[f]BEARPEX09 (Jun-Jul 2009)	[g]SOAS (Jun-Jul 2013)	GoAmazon (Feb-Mar 2014)
Analytical Technique	LIF	LIF	LIF	[h]LIF	[h]LIF	[h]LIF	[h]LIF	CIMS
Averaged Time (LST)	14:00 - 17:00	10:00 - 11:00	11:00 -12:00	11:00 – 14:00	12:00 – 16:00	09:00 - 15:00	10:00 -15:00	10:00 - 15:00
CO (ppb)	122	260	111	260	540	130	134	121
OH (molec cm^{-3})	4.4×10^6	3.6×10^6	2.2×10^6	1.3×10^6	6.9×10^6	1.3×10^6	1.2×10^6	$1.0 \times 10^6 \pm 0.6 \times 10^6$
Isoprene (ppb)	4.3	1.86	2	1	0.84	1.7	5.14	2.25
MVK+MACR (ppb)	1.6	0.34	0.21	0.5	0.71	0.79	1.41	1.34
NO (ppt)	13	80	40	50	250	74	42	[i]27 ± 25
NO_2 (ppt)		456	130	220	3300	200	293	[i]85 ± 50
O_3 (ppb)	17	41	12.5	30	93	54	37	21
OH reactivity (s^{-1})	19	11	19.8	12	11	18.5	21.1	8.5 ± 1.4

[a] Tropical forest in Suriname, Guyana and Guyane (Lelieveld et al., 2008)
[b] Deciduous forest in northern Michigan (D. Tan et al., 2001)
[c] Danum Valley in the Sabah region of a Borneo forest (Whalley et al., 2011)
[d] Deciduous forest in northern Michigan (Griffith et al., 2013)
[e] Botanical garden in a rural site in Wangdu, North China Plain (Z. Tan et al., 2017)
[f] Ponderosa pine plantation in the California Sierra Nevada Mountains (Mao et al., 2012)
[g] Talladega National Forest in Brent, Alabama (Feiner et al., 2016)
[h] Chemical removal method for determining background OH conducted during the observation period or tested out after the campaign.
[I] NO_2 was estimated as 6 % of observed NO_Y and NO is averaged from box model simulations with the MCM v3.3.1

References

Alaghmand, M., Shepson, P. B., Starn, T. K., Jobson, B. T., Wallace, H. W., Carroll, M. A., … Keutsch, F. (2011). The Morning NOxmaximum in the forest atmosphere boundary layer. *Atmospheric Chemistry and Physics Discussions*, *11*(10), 29251–29282. https://doi.org/10.5194/acpd-11-29251-2011

Archibald, A. T., Cooke, M. C., Utembe, S. R., Shallcross, D. E., Derwent, R. G., & Jenkin, M. E. (2010). Impacts of mechanistic changes on HOx formation and recycling in the oxidation of isoprene. *Atmospheric Chemistry and Physics*, *10*(17), 8097–8118. https://doi.org/10.5194/acp-10-8097-2010

Asatryan, R., Da Silva, G., & Bozzelli, J. W. (2010). Quantum chemical study of the acrolein (CH2CHCHO) + OH + O2 reactions. *Journal of Physical Chemistry A*, *114*(32), 8302–8311. research-article. https://doi.org/10.1021/jp104828a

Bakwin, P. S., Wofsy, S. C., & Fan, S. (1990). Measurements of Reactive Nitrogen Oxides (NOy) Within and above a Tropical Forest Canopy in the Wet Season. *Journal of Geophysical Research*, *95*(D10), 16765–16772.

Bates, K. H., & Jacob, D. J. (2019). A new model mechanism for atmospheric oxidation of isoprene: Global effects on oxidants, nitrogen oxides, organic products, and secondary organic aerosol. *Atmospheric Chemistry and Physics*, *19*(14), 9613–9640. https://doi.org/10.5194/acp-19-9613-2019

Berndt, T., Hyttinen, N., Herrmann, H., & Hansel, A. (2019). First oxidation products from the reaction of hydroxyl radicals with isoprene for pristine environmental conditions. *Communications Chemistry*, *2*(1). https://doi.org/10.1038/s42004-019-0120-9

Butler, T. M., Taraborrelli, D., Brühl, C., Fischer, H., Harder, H., Martinez, M., … Lelieveld, J. (2008). Improved simulation of isoprene oxidation chemistry with the ECHAM5/MESSy chemistry-climate model: lessons from the GABRIEL airborne field campaign. *Atmospheric Chemistry and Physics*, *8*, 4529–4546.

Carslaw, N., Creasey, D. J., Harrison, D., Heard, D. E., Hunter, M. C., Jacobs, P. J., … Seakins, P. W. (2001). OH and HO 2 radical chemistry in a forested region of north-western Greece. *Atmospheric Environment*, *35*(27), 4725–4737. https://doi.org/10.1016/S1352-2310(01)00089-9

Chen, Q., Fan, J., Hagos, S., Gustafson, W. I., & Berg, L. K. (2015). Roles of wind shear at different vertical levels: Cloud system organization and properties. *Journal of Geophysical Research Atmospheres*, *120*(13), 6551–6574. https://doi.org/10.1002/2015JD023253

Chen, S., Ren, X., Mao, J., Chen, Z., Brune, W. H., Lefer, B., … Crawford, J. H. (2010). A comparison of chemical mechanisms based on TRAMP-2006 field data. *Atmospheric Environment*, *44*(33), 4116–4125. https://doi.org/10.1016/j.atmosenv.2009.05.027

Crounse, J. D., Knap, H. C., Ørnsø, K., Jørgensen, S., Paulot, F., Kjaergaard, H. G., & Wennberg, P. O. (2012). Atmospheric fate of methacrolein. 1. Peroxy radical isomerization following addition of oh and O 2. *Journal of Physical Chemistry A*, *116*(24), 5756–5762. https://doi.org/10.1021/jp211560u

Crounse, J. D., Paulot, F., Kjaergaard, H. G., & Wennberg, P. O. (2011). Peroxy radical

isomerization in the oxidation of isoprene. *Physical Chemistry Chemical Physics*, *13*(30), 13607. https://doi.org/10.1039/c1cp21330j

Crounse, J. D., Teng, A., and Wennberg, P. O.: Experimental constrains on the distribution and fate of peroxy radicals formed in the reactions of isoprene + OH + O_2 presented at the Atmospheric Chemical Mechanisms: Simple Models – Real world Complexities, Universtiy of California, Davis, USA, 10–12 December 2014.

Dodge, M. C. (2000). Chemical oxidant mechanisms for air quality modeling: Critical review. *Atmospheric Environment*, *34*(12–14), 2103–2130. https://doi.org/10.1016/S1352-2310(99)00461-6

Feiner, P. A., Brune, W. H., Miller, D. O., Zhang, L., Cohen, R. C., Romer, P. S., … Fry, J. L. (2016). Testing atmospheric oxidation in an Alabama forest. *Journal of the Atmospheric Sciences*, *73*(12), 4699–4710. https://doi.org/10.1175/JAS-D-16-0044.1

Flynn, C. J. (2016). *Shortwave Array Spectroradiometer–Hemispheric (SASHe) Instrument Handbook*. United States: N. p. https://doi.org/10.2172/1251414

Fuchs, H., Hofzumahaus, A., Rohrer, F., Bohn, B., Brauers, T., Dorn, H.-P., … Wahner, A. (2013). Experimental evidence for efficient hydroxyl radical regeneration in isoprene oxidation. *Nature Geoscience*, *6*(12), 1023–1026. https://doi.org/10.1038/ngeo1964

Fuchs, H., Tan, Z., Hofzumahaus, A., Broch, S., Dorn, H. P., Holland, F., … Wahner, A. (2016). Investigation of potential interferences in the detection of atmospheric ROx radicals by laser-induced fluorescence under dark conditions. *Atmospheric Measurement Techniques*, *9*(4), 1431–1447. https://doi.org/10.5194/amt-9-1431-2016

Goliff, W. S., Stockwell, W. R., & Lawson, C. V. (2013). The regional atmospheric chemistry mechanism, version 2. *Atmospheric Environment*, *68*, 174–185. https://doi.org/10.1016/j.atmosenv.2012.11.038

Graus, M., Muller, M., & Hansel, A. (2010). High resolution PTR-TOF: Quantification and Formula Confirmation of VOC in Real Time. *Journal of the American Society for Mass Spectrometry*, *21*(6), 1037–1044. https://doi.org/10.1016/j.jasms.2010.02.006

Greenberg, J. P., & Zimmerman, P. R. (1984). Nonmethane hydrocarbons in remote tropical, continental, and marine atmospheres. *Journal of Geophysical Research*, *89*(D3), 4767–4778. https://doi.org/10.1029/JD089iD03p04767

Griffith, S. M., Hansen, R. F., Dusanter, S., Stevens, P. S., Alaghmand, M., Bertman, S. B., … Zhou, X. L. (2013). OH and HO2 radical chemistry during PROPHET 2008 and CABINEX 2009 - Part 1: Measurements and model comparison. *Atmospheric Chemistry and Physics*, *13*(11), 5403–5423. https://doi.org/10.5194/acp-13-5403-2013

Gross, A., & Stockwell, W. R. (2003). Comparison of the EMEP, RADM2 and RACM mechanisms. *Journal of Atmospheric Chemistry*, *44*(2), 151–170. https://doi.org/10.1023/A:1022483412112

Hens, K., Novelli, A., Martinez, M., Auld, J., Axinte, R., Bohn, B., … Harder, H. (2014). Observation and modelling of HOx radicals in a boreal forest. *Atmospheric Chemistry and Physics*, *14*(16), 8723–8747. https://doi.org/10.5194/acp-14-8723-2014

Hofzumahaus, A., Rohrer, F., Lu, K., Bohn, B., Brauers, T., Chang, C., … Zhang, Y. (2009).

Amplified Trace Gas Removal in the Troposphere. *Science*, *324*, 1702–1704. https://doi.org/10.1126/science.1164566

Holland, F., Hofzumahaus, A., Schäfer, J., Kraus, A., & Pätz, H. W. (2003). Measurements of OH and HO2 radical concentrations and photolysis frequencies during BERLIOZ. *Journal of Geophysical Research: Atmospheres*, *108*(4). https://doi.org/10.1029/2001jd001393

Huey, L. G. (2007). Measurement of trace atmospheric species by chemical ionization mass spectrometry: Speciation of reactive nitrogen and future directions. *Mass Spectrometry Reviews*. https://doi.org/10.1002/mas.20118

Jacob, J., & Wofsy, S. C. (1988). Photochemistry of biogenic emissions over the Amazon Forest. *Journal of Geophysical Research*, *93*(D2), 1477–1486.

Jenkin, M. E., Hurley, M. D., & Wallington, T. J. (2007). Investigation of the radical product channel of the CH3C(O)O2 + HO2 Reaction in the Gas Phase. *Physical Chemistry Chemical Physics*, *9*(24), 3149–3162. https://doi.org/10.1039/b702757e

Jenkin, M. E., Hurley, M. D., & Wallington, T. J. (2010). Investigation of the radical product channel of the CH3OCH 2O2 + HO2 Reaction in the Gas Phase. *Journal of Physical Chemistry A*, *114*(1), 408–416. https://doi.org/10.1021/jp908158w

Jenkin, M. E., Young, J. C., & Rickard, A. R. (2015). The MCM v3.3.1 degradation scheme for isoprene. *Atmospheric Chemistry and Physics*, *15*(20), 11433–11459. https://doi.org/10.5194/acp-15-11433-2015

Jeong, D., Seco, R., Gu, D., Lee, Y., Nault, B. A., Knote, C. J., … Kim, S. (2019). Integration of Airborne and Ground Observations of Nitryl Chloride in the Seoul Metropolitan Area and the Implications on Regional Oxidation Capacity During KORUS-AQ 2016. *Atmospheric Chemistry and Physics*, *19*, 12779–12795. https://doi.org/10.5194/acp-2018-1216

Jimenez, P., Baldasano, J. M., & Dabdub, D. (2003). Comparison of photochemical mechanisms for air quality modeling. *Atmospheric Environment*, *37*(30), 4179–4194. https://doi.org/10.1016/S1352-2310(03)00567-3

Jordan, A., Haidacher, S., Hanel, G., Hartungen, E., Märk, L., Seehauser, H., … Märk, T. D. (2009). A high resolution and high sensitivity proton-transfer-reaction time-of-flight mass spectrometer (PTR-TOF-MS). *International Journal of Mass Spectrometry*, *286*(2–3), 122–128. https://doi.org/10.1016/j.ijms.2009.07.005

Kaiser, J., Skog, K. M., Baumann, K., Bertman, S. B., Brown, S. B., Brune, W. H., … Keutsch, F. N. (2016). Speciation of OH reactivity above the canopy of an isoprene-dominated forest. *Atmospheric Chemistry and Physics*, *16*(14), 9349–9359. https://doi.org/10.5194/acp-16-9349-2016

Kim, S., Guenther, A., Lefer, B., Flynn, J., Griffin, R., Rutter, A. P., … Cevik, B. K. (2015). Potential role of stabilized criegee radicals in sulfuric acid production in a high biogenic VOC environment. *Environmental Science and Technology*, *49*(6), 3383–3391. https://doi.org/10.1021/es505793t

Kim, S., Kim, S. Y., Lee, M., Shim, H., Wolfe, G. M., Guenther, A. B., … Han, J. (2015). Impact of isoprene and HONO chemistry on ozone and OVOC formation in a semirural South Korean forest. *Atmospheric Chemistry and Physics*, *15*(8), 4357–4371.

https://doi.org/10.5194/acp-15-4357-2015

Kim, S., Sanchez, D., Wang, M., Seco, R., Jeong, D., Hughes, S., … Hong, J. (2016). OH reactivity in urban and suburban regions in Seoul, South Korea-an East Asian megacity in a rapid transition. *Faraday Discussions*, *189*, 231–251. https://doi.org/10.1039/c5fd00230c

Knote, C., Hodzic, A., Jimenez, J. L., Volkamer, R., Orlando, J. J., Baidar, S., … Zhang, Q. (2014). Simulation of semi-explicit mechanisms of SOA formation from glyoxal in aerosol in a 3-D model. *Atmospheric Chemistry and Physics*, *14*(12), 6213–6239. https://doi.org/10.5194/acp-14-6213-2014

Knote, C., Tuccella, P., Curci, G., Emmons, L., Orlando, J. J., Madronich, S., … Zhang, Y. (2015). Influence of the choice of gas-phase mechanism on predictions of key gaseous pollutants during the AQMEII phase-2 intercomparison. *Atmospheric Environment*, *115*, 553–568. https://doi.org/10.1016/j.atmosenv.2014.11.066

Kubistin, D., Harder, H., Martinez, M., Rudolf, M., Sander, R., Bozem, H., … Lelieveld, J. (2010). Hydroxyl radicals in the tropical troposphere over the Suriname rainforest: Comparison of measurements with the box model MECCA. *Atmospheric Chemistry and Physics*, *10*(19), 9705–9728. https://doi.org/10.5194/acp-10-9705-2010

Kuhn, M., Builtjes, P. J. H., Poppe, D., Simpson, D., Stockwell, W. R., Andersson-Sköld, Y., … Vogel, H. (1998). Intercomparison of the gas-phase chemistry in several chemistry and transport models. *Atmospheric Environment*, *32*(4), 693–709. https://doi.org/10.1016/S1352-2310(97)00329-4

Kürten, A., Rondo, L., Ehrhart, S., & Curtius, J. (2011). Performance of a corona ion source for measurement of sulfuric acid by chemical ionization mass spectrometry. *Atmospheric Measurement Techniques*, *4*(3), 437–443. https://doi.org/10.5194/amt-4-437-2011

Lelieveld, J., Butler, T. M., Crowley, J. N., Dillon, T. J., Fischer, H., Ganzeveld, L., … Williams, J. (2008). Atmospheric oxidation capacity sustained by a tropical forest. *Nature*, *452*(7188), 737–740. https://doi.org/10.1038/nature06870

Levy, H. (1971). Normal Atmosphere: Large Radical and Formaldehyde Concentrations Predicted. *Science*, *173*(3992), 141–143. https://doi.org/10.1126/science.173.3992.141

Liao, J., Huey, L. G., Liu, Z., Tanner, D. J., Cantrell, C. A., Orlando, J. J., … Nowak, J. B. (2014). High levels of molecular chlorine in the Arctic atmosphere. *Nature Geoscience*, *7*(2), 91–94. https://doi.org/10.1038/ngeo2046

Liao, J., Huey, L. G., Tanner, D. J., Brough, N., Brooks, S., Dibb, J. E., … Gorham, K. (2011). Observations of hydroxyl and peroxy radicals and the impact of BrO at Summit, Greenland in 2007 and 2008. *Atmospheric Chemistry and Physics*, *11*(16), 8577–8591. https://doi.org/10.5194/acp-11-8577-2011

Liao, J., Huey, L. G., Tanner, D. J., Flocke, F. M., Orlando, J. J., Neuman, J. A., … Stephens, C. R. (2012). Observations of inorganic bromine (HOBr, BrO, and Br2) speciation at Barrow, Alaska, in spring 2009. *Journal of Geophysical Research Atmospheres*, *117*(6), 1–11. https://doi.org/10.1029/2011JD016641

Liu, Y., Brito, J., Dorris, M. R., Rivera-Rios, J. C., Seco, R., Bates, K. H., … Martin, S. T. (2016). Isoprene photochemistry over the Amazon rainforest. *Proceedings of the National*

Academy of Sciences, *113*(22), 6125–6130. https://doi.org/10.1073/pnas.1524136113

Liu, Y., Seco, R., Kim, S., Guenther, A. B., Goldstein, A. H., Keutsch, F. N., … Martin, S. T. (2018). Isoprene photo-oxidation products quantify the effect of pollution on hydroxyl radicals over Amazonia. *Science Advances*, *4*(4), 1–9. https://doi.org/10.1126/sciadv.aar2547

Logan, J. A., Prather, M. J., Wofsy, S. C., & Mc Elroy, M. B. (1981). Tropospheric chemistry: A global perspective. *Journal of Geophysical Research*. https://doi.org/10.1029/JC086iC08p07210

Madronich, S., & Flocke, S. (1998). Handbook of Environmental Chemistry. In *Handbook of Environmental Chemistry* (P. Boule, pp. 1–26). Heidelberg: Springer_Verlag.

Mao, J., Ren, X., Zhang, L., Van Duin, D. M., Cohen, R. C., Park, J. H., … Brune, W. H. (2012). Insights into hydroxyl measurements and atmospheric oxidation in a California forest. *Atmospheric Chemistry and Physics*, *12*(17), 8009–8020. https://doi.org/10.5194/acp-12-8009-2012

Martin, S. T., Artaxo, P., MacHado, L. A. T., Manzi, A. O., Souza, R. A. F., Schumacher, C., … Wendisch, M. (2016). Introduction: Observations and Modeling of the Green Ocean Amazon (GoAmazon2014/5). *Atmospheric Chemistry and Physics*, *16*(8), 4785–4797. https://doi.org/10.5194/acp-16-4785-2016

Martin, S. T., Artaxo, P., Machado, L., Manzi, A. O., Souza, R. A. F., Schumacher, C., … Wendisch, M. (2017). The Green Ocean Amazon Experiment (GoAmazon2014/5) Observes Pollution Affecting Gases, Aerosols, Clouds, and Rainfall over the Rain Forest. *Bulletin of the American Meteorological Society*, (MAY), BAMS-D-15-00221.1. https://doi.org/10.1175/BAMS-D-15-00221.1

Mauldin, R. L., Frost, G. J., Chen, G., Tanner, D. J., Prevot, A. S. H., Davis, D. D., & Eisele, F. L. (1998). OH measurements during the First Aerosol Characterization Experiment (ACE 1): Observations and model comparisons. *Journal of Geophysical Research Atmospheres*, *103*(D13), 16713–16729. https://doi.org/10.1029/98JD00882

Mauldin, R. L., Kosciuch, E., Henry, B., Eisele, F. L., Shetter, R., Lefer, B., … Tanner, D. (2010). Measurements of OH, HO2+RO2,H2SO4, and MSA at the South Pole during ISCAT 2000. *Advances in Horticultural Science*, *24*(1), 43–52. https://doi.org/10.1016/j.atmosenv.2004.06.031

Nolscher, A. C., Yanez-Serrano, A. M., Wolff, S., Carioca de Araujo, A., Lavric, J. V., Kesselmeier, J., Williams, J. (2016). Unexpected seasonality in quantity and composition of Amazon rainforest air reactivity. Nature Communications, 7 (10383). https://doi.org/10.1038/ncomms10383

Novelli, A., Hens, K., Ernest, C. T., Martinez, M., Nölscher, A. C., Sinha, V., … Harder, H. (2017). Estimating the atmospheric concentration of Criegee intermediates and their possible interference in a FAGE-LIF instrument. *Atmospheric Chemistry and Physics*, *17*(12), 7807–7826. https://doi.org/10.5194/acp-17-7807-2017

Novelli, A., Hens, K., Tatum Ernest, C., Kubistin, D., Regelin, E., Elste, T., … Harder, H. (2014). Characterisation of an inlet pre-injector laser-induced fluorescence instrument for the measurement of atmospheric hydroxyl radicals. *Atmospheric Measurement Techniques*,

7(10), 3413–3430. https://doi.org/10.5194/amt-7-3413-2014

Novelli, A., Kaminski, M., Rolletter, M., Acir, I. H., Bohn, B., Dorn, H. P., … Fuchs, H. (2018). Evaluation of OH and HO2 concentrations and their budgets during photooxidation of 2-methyl-3-butene-2-ol (MBO) in the atmospheric simulation chamber SAPHIR. *Atmospheric Chemistry and Physics*, *18*(15), 11409–11422. https://doi.org/10.5194/acp-18-11409-2018

Novelli, A., Vereecken, L., Bohn, B., Dorn, H. P., Gkatzelis, G. I., Hofzumahaus, A., … Fuchs, H. (2020). Importance of isomerization reactions for OH radical regeneration from the photo-oxidation of isoprene investigated in the atmospheric simulation chamber SAPHIR. *Atmospheric Chemistry and Physics*, *20*(6), 3333–3355. https://doi.org/10.5194/acp-20-3333-2020

Peeters, J.: Interactive comment on "The MCM v3.3. degradation scheme for isoprene" by M. E. Jenkin et al., Atmos. Chem. Phys. Discuss., 15, C2486–C2486, 2015.

Peeters, J., & Müller, J. F. (2010). HOx radical regeneration in isoprene oxidation via peroxy radical isomerisations. II: experimental evidence and global impact. *Physical Chemistry Chemical Physics*, *12*(42), 14227. https://doi.org/10.1039/c0cp00811g

Peeters, J., Müller, J. F., Stavrakou, T., & Nguyen, V. S. (2014). Hydroxyl radical recycling in isoprene oxidation driven by hydrogen bonding and hydrogen tunneling: The upgraded LIM1 mechanism. *Journal of Physical Chemistry A*, *118*(38), 8625–8643. https://doi.org/10.1021/jp5033146

Peeters, J., Nguyen, T. L., & Vereecken, L. (2009). HOx radical regeneration in the oxidation of isoprene. *Physical Chemistry Chemical Physics*, *11*(28), 5935. https://doi.org/10.1039/b908511d

Pugh, T. A. M., MacKenzie, A. R., Hewitt, C. N., Langford, B., Edwards, P. M., Furneaux, K. L., … Whalley, L. K. (2010). Simulating atmospheric composition over a South-East Asian tropical rainforest: Performance of a chemistry box model. *Atmospheric Chemistry and Physics*, *10*, 279–298. https://doi.org/10.5194/acpd-9-19243-2009

Raso, A. R. W., Custard, K. D., May, N. W., Tanner, D., Newburn, M. K., Walker, L., … Pratt, K. A. (2017). Active molecular iodine photochemistry in the Arctic. *Proceedings of the National Academy of Sciences*, *114*(38), 10053–10058. https://doi.org/10.1073/pnas.1702803114

Ren, X., Olson, J. R., Crawford, J. H., Brune, W. H., Mao, J., Long, R. B., … Shetter, R. E. (2008). HOx chemistry during INTEX-A 2004: Observation, model calculation, and comparison with previous studies. *Journal of Geophysical Research Atmospheres*, *113*(5), 1–13. https://doi.org/10.1029/2007JD009166

Rickly, P., & Stevens, P. S. (2018). Measurements of a potential interference with laser-induced fluorescence measurements of ambient OH from the ozonolysis of biogenic alkenes. *Atmospheric Measurement Techniques*, *11*(1), 1–16. https://doi.org/10.5194/amt-11-1-2018

Rohrer, F., Lu, K., Hofzumahaus, A., Bohn, B., Brauers, T., Chang, C. C., … Wahner, A. (2014). Maximum efficiency in the hydroxyl-radical-based self-cleansing of the troposphere. *Nature Geoscience*, *7*(8), 559–563. https://doi.org/10.1038/ngeo2199

Ruiz, L. H., & Yarwood, G. (2013). *Prepared for the Texas AQRP (Project 12-012) University*

of Texas at Austin, and ENVIRON International Corporation; Novato, CA: 2013. Interactions between organic aerosol and NOy: Influence on oxidant production.

Sanchez, D., Jeong, D., Seco, R., Wrangham, I., Park, J. H., Brune, W. H., … Kim, S. (2018). Intercomparison of OH and OH reactivity measurements in a high isoprene and low NO environment during the Southern Oxidant and Aerosol Study (SOAS). *Atmospheric Environment*, *174*, 227–236. https://doi.org/10.1016/j.atmosenv.2017.10.056

Saunders, S. M., Jenkin, M. E., Derwent, R. G., & Pilling, M. J. (1997). World Wide Web site of a master chemical mechanism (MCM) for use in tropospheric chemistry models. *Atmospheric Environment*, *31*(8), 1249. https://doi.org/10.1016/S1352-2310(97)85197-7

Saunders, S. M., Jenkin, M. E., Derwent, R. G., & Pilling, M. J. (2003). Protocol for the development of the Master Chemical Mechanism, MCM v3 (Part A): tropospheric degradation of non-aromatic volatile organic compounds. *Atmospheric Chemistry and Physics*, *3*(1), 161–180. https://doi.org/10.5194/acp-3-161-2003

Sjostedt, S. J., Huey, L. G., Tanner, D. J., Peischl, J., Chen, G., Dibb, J. E., … Stohl, A. (2007). Observations of hydroxyl and the sum of peroxy radicals at Summit, Greenland during summer 2003. *Atmospheric Environment*, *41*(24), 5122–5137. https://doi.org/10.1016/j.atmosenv.2006.06.065

Stone, D., Evans, M. J., Commane, R., Ingham, T., Floquet, C. F. A., McQuaid, J. B., … Heard, D. E. (2010). HOx observations over West Africa during AMMA: Impact of isoprene and NOx. *Atmospheric Chemistry and Physics*, *10*(19), 9415–9429. https://doi.org/10.5194/acp-10-9415-2010

Tan, D., Faloona, I., Simpas, J. B., Brune, W., Shepson, P. B., Couch, T. L., … Stockwell, W. (2001). HOx budgets in a deciduous forest: Results from the PROPHET summer 1998 campaign. *Journal of Geophysical Research: Atmospheres*, *106*(D20), 24407–24427. https://doi.org/10.1029/2001JD900016

Tan, Z., Fuchs, H., Lu, K., Hofzumahaus, A., Bohn, B., Broch, S., … Zhang, Y. (2017). Radical chemistry at a rural site (Wangdu) in the North China Plain: Observation and model calculations of OH, HO2 and RO2 radicals. *Atmospheric Chemistry and Physics*, *17*(1), 663–690. https://doi.org/10.5194/acp-17-663-2017

Tanner, D. J., Jefferson, A., & Eisele, F. L. (1997). Selected Ion Chemical Ionization Mass Spectrometric Measurement of OH. *Journal Of Geophysical Research-Atmospheres*, *102*(D5), 6415–6425. https://doi.org/Doi 10.1029/96jd03919

Taraborrelli, D., Lawrence, M. G., Butler, T. M., Sander, R., & Lelieveld, J. (2009). Mainz Isoprene Mechanism 2 (MIM2): An isoprene oxidation mechanism for regional and global atmospheric modelling. *Atmospheric Chemistry and Physics*, *9*(8), 2751–2777. https://doi.org/10.5194/acp-9-2751-2009

Teng, A. P., Crounse, J. D., & Wennberg, P. O. (2017). Isoprene Peroxy Radical Dynamics. *Journal of the American Chemical Society*, *139*(15), 5367–5377. https://doi.org/10.1021/jacs.6b12838

Thornton, J. A., Wooldridge, P. J., Cohen, R. C., Martinez, M., Harder, H., Brune, W. H., … Fried, A. (2002). Ozone production rates as a function of NOx abundances and HOx production rates in the Nashville urban plume. *Journal of Geophysical Research*, *107*(D12),

4146. https://doi.org/10.1029/2001JD000932

Wennberg, P. O., Bates, K. H., Crounse, J. D., Dodson, L. G., McVay, R. C., Mertens, L. A., … Seinfeld, J. H. (2018). Gas-Phase Reactions of Isoprene and Its Major Oxidation Products. *Chemical Reviews*, *118*(7), 3337–3390. https://doi.org/10.1021/acs.chemrev.7b00439

Whalley, L. K., Edwards, P. M., Furneaux, K. L., Goddard, A., Ingham, T., Evans, M. J., … Heard, D. E. (2011). Quantifying the magnitude of a missing hydroxyl radical source in a tropical rainforest. *Atmospheric Chemistry and Physics*, *11*(14), 7223–7233. https://doi.org/10.5194/acp-11-7223-2011

Wolfe, G. M., Cantrell, C., Kim, S., Mauldin, R. L., Karl, T., Harley, P., … Keutsch, F. N. (2014). Missing peroxy radical sources within a summertime ponderosa pine forest. *Atmospheric Chemistry and Physics*, *14*(9), 4715–4732. https://doi.org/10.5194/acp-14-4715-2014

Wolfe, G. M., Crounse, J. D., Parrish, J. D., St. Clair, J. M., Beaver, M. R., Paulot, F., … Keutsch, F. N. (2012). Photolysis, OH reactivity and ozone reactivity of a proxy for isoprene-derived hydroperoxyenals (HPALDs). *Physical Chemistry Chemical Physics*, *14*(20), 7276–7286. https://doi.org/10.1039/c2cp40388a

Wolfe, G. M., Kaiser, J., Hanisco, T. F., Keutsch, F. N., De Gouw, J. A., Gilman, J. B., … Warneke, C. (2016). Formaldehyde production from isoprene oxidation across NOx regimes. *Atmospheric Chemistry and Physics*, *16*(4), 2597–2610. https://doi.org/10.5194/acp-16-2597-2016

Wolfe, G. M., Marvin, M. R., Roberts, S. J., Travis, K. R., & Liao, J. (2016). The framework for 0-D atmospheric modeling (F0AM) v3.1. *Geoscientific Model Development*, *9*(9), 3309–3319. https://doi.org/10.5194/gmd-9-3309-2016

Yarwood, G., Whitten, G., & Rao, S. (2005). *Updates to the Carbon Bond 4 photochemical mechanism Prepared for Lake Michigan Air Directors consortium*.

Zimmerman, P. R., Greenberg, J. P., & Westberg, C. E. (1988). Measurements of atmospheric hydrocarbons and biogenic emission fluxes in the Amazon Boundary layer. *Journal of Geophysical Research: Atmospheres*, *93*(D2), 1407–1416. https://doi.org/10.1029/JD093iD02p01407

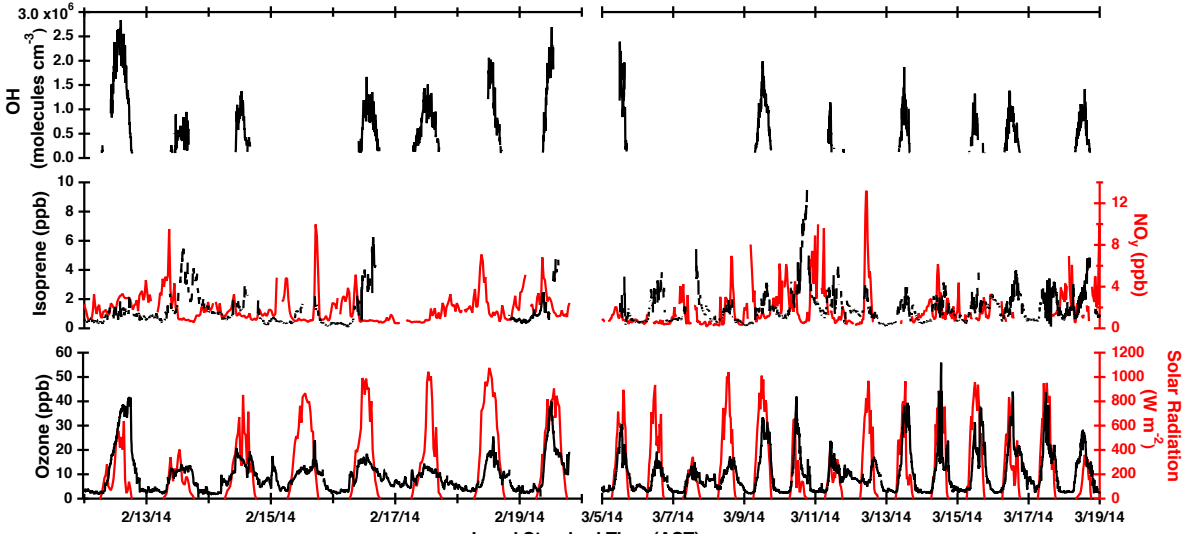
3.0 x10^6
OH (molecules cm^-3)
2.5
2.0
1.5
1.0
0.5
0.0
Isoprene (ppb)
10
8
6
4
2
0
NOy (ppb)
12
8
4
0
Ozone (ppb)
60
50
40
30
20
10
0
Solar Radiation (W m^-2)
1200
1000
800
600
400
200
0
2/13/14
2/15/14
2/17/14
2/19/14
3/5/14
3/7/14
3/9/14
3/11/14
3/13/14
3/15/14
3/17/14
3/19/14
Local Standard Time (AST)

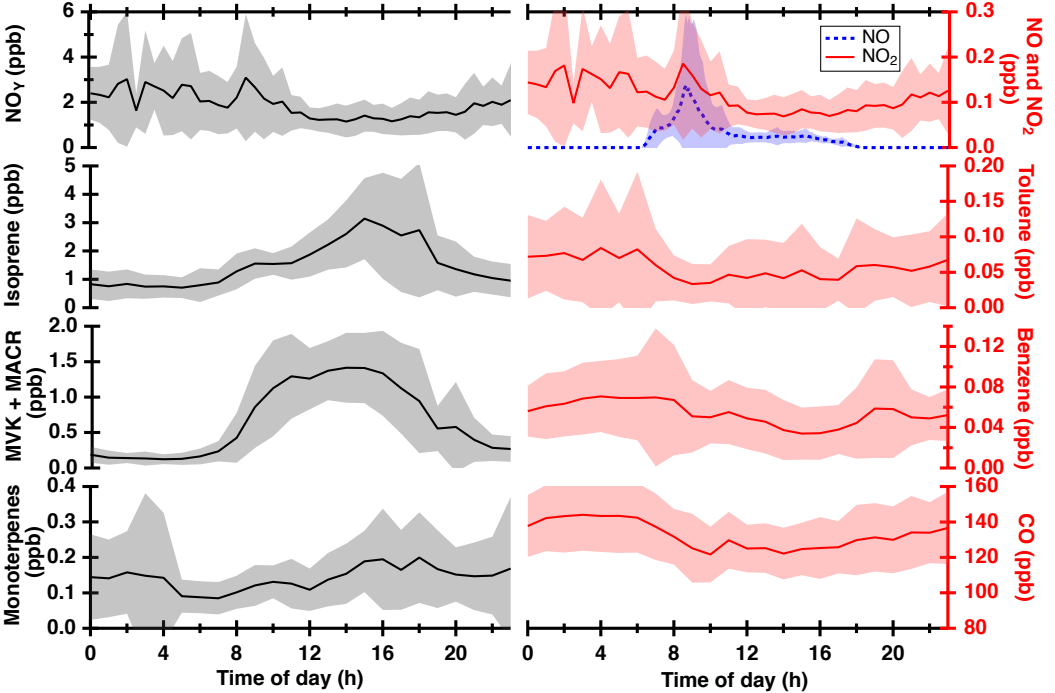
NO$_Y$ (ppb)
Isoprene (ppb)
MVK + MACR (ppb)
Monoterpenes (ppb)
NO
NO$_2$
NO and NO$_2$ (ppb)
Toluene (ppb)
Benzene (ppb)
CO (ppb)
Time of day (h)
Time of day (h)

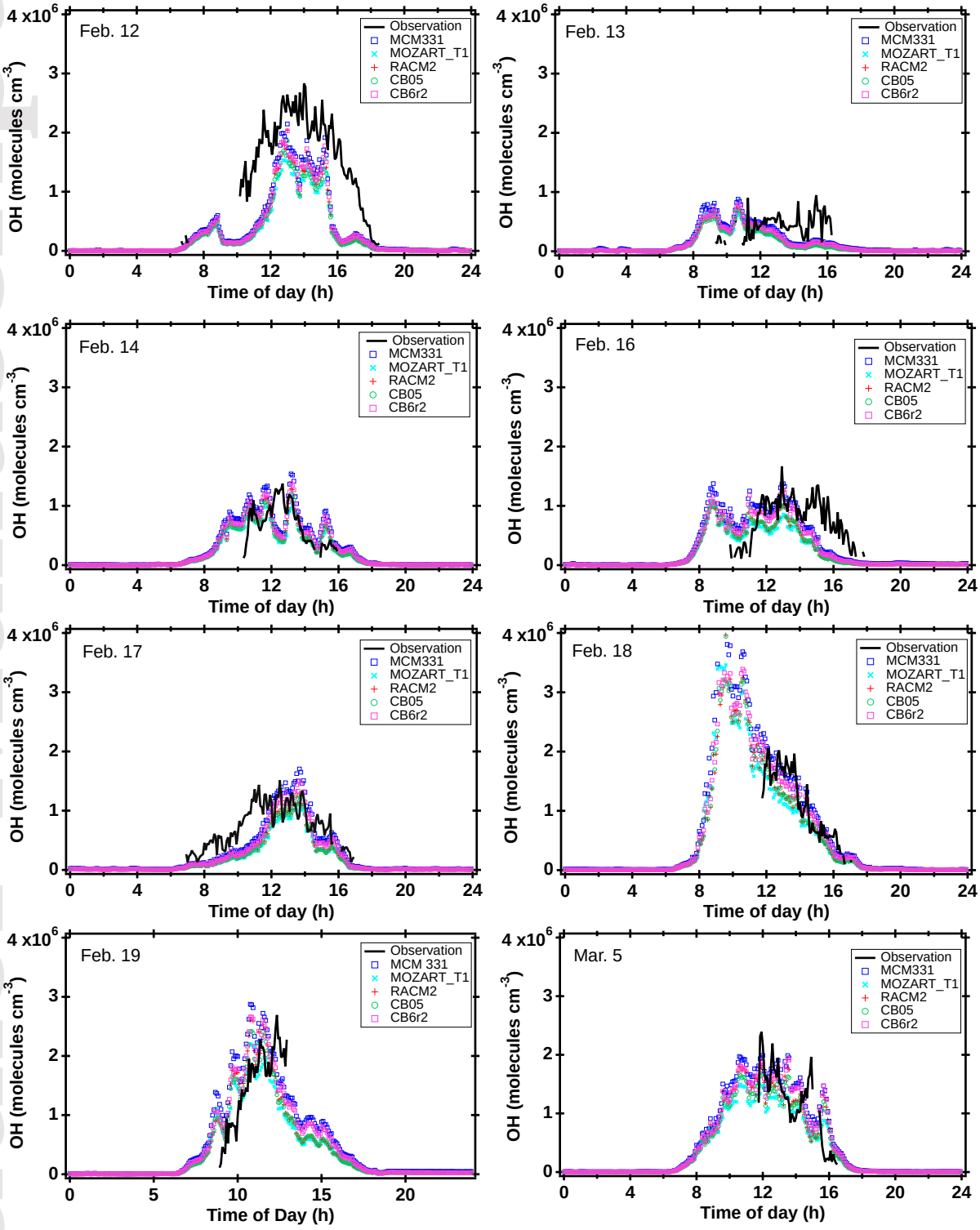

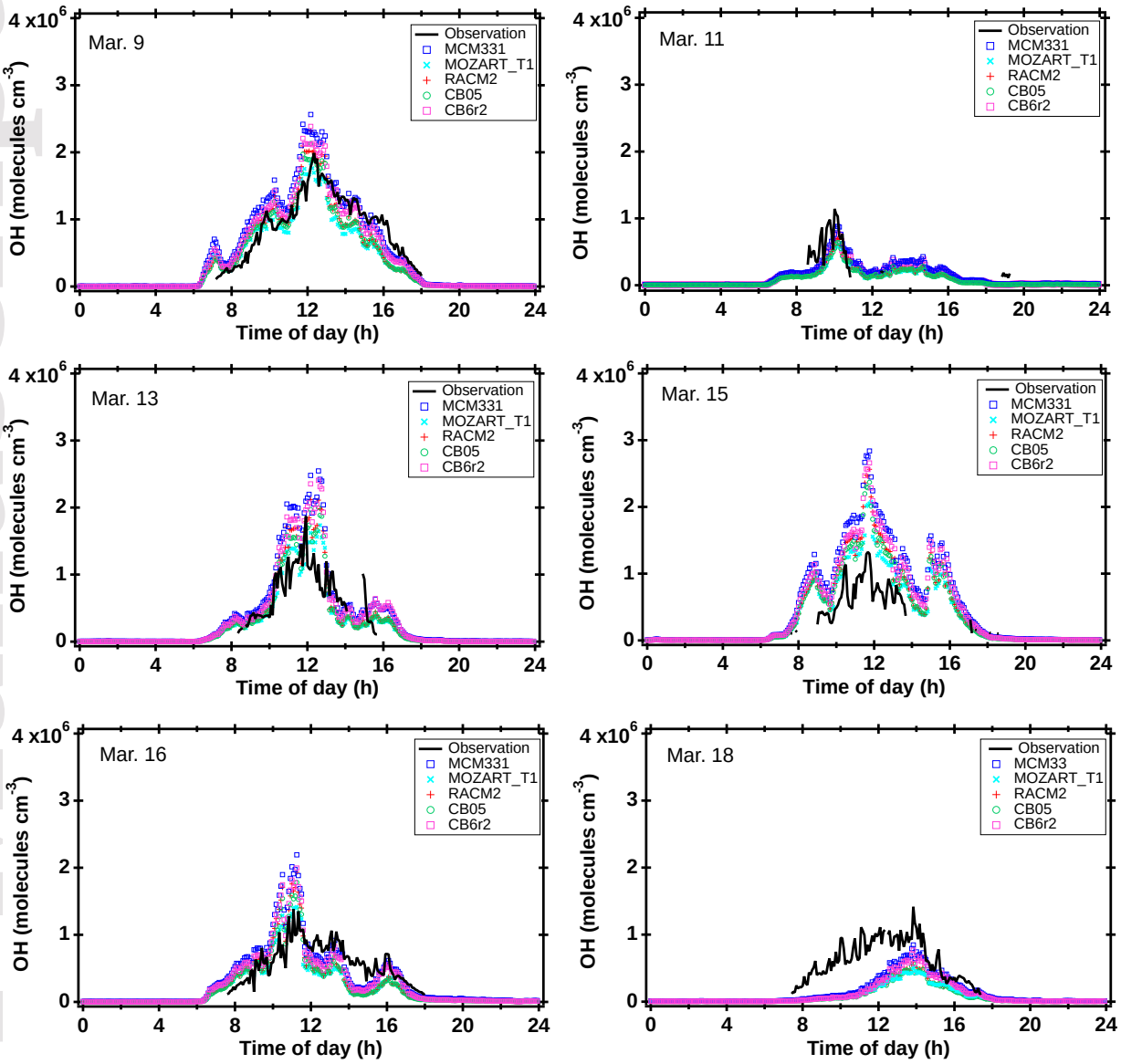

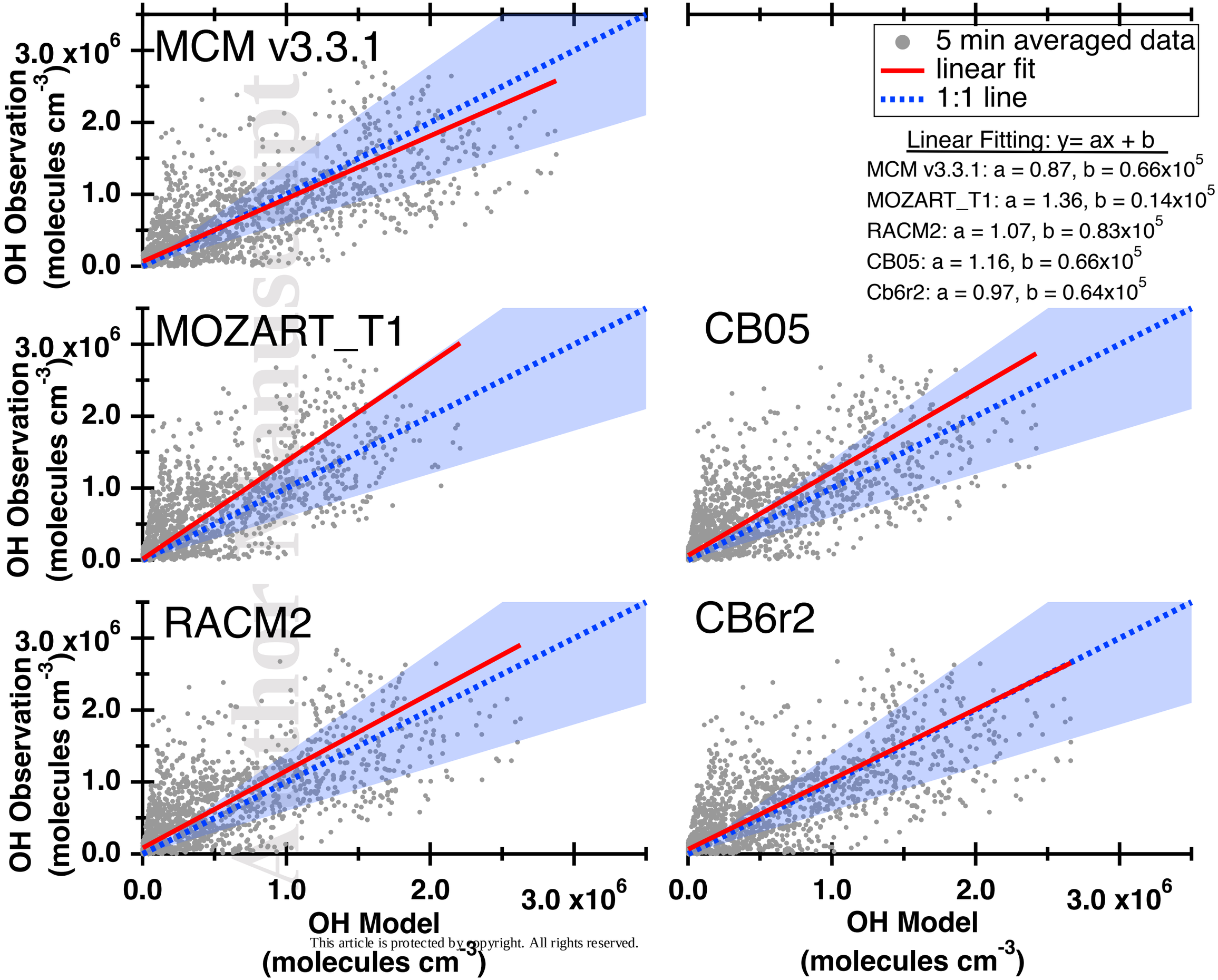

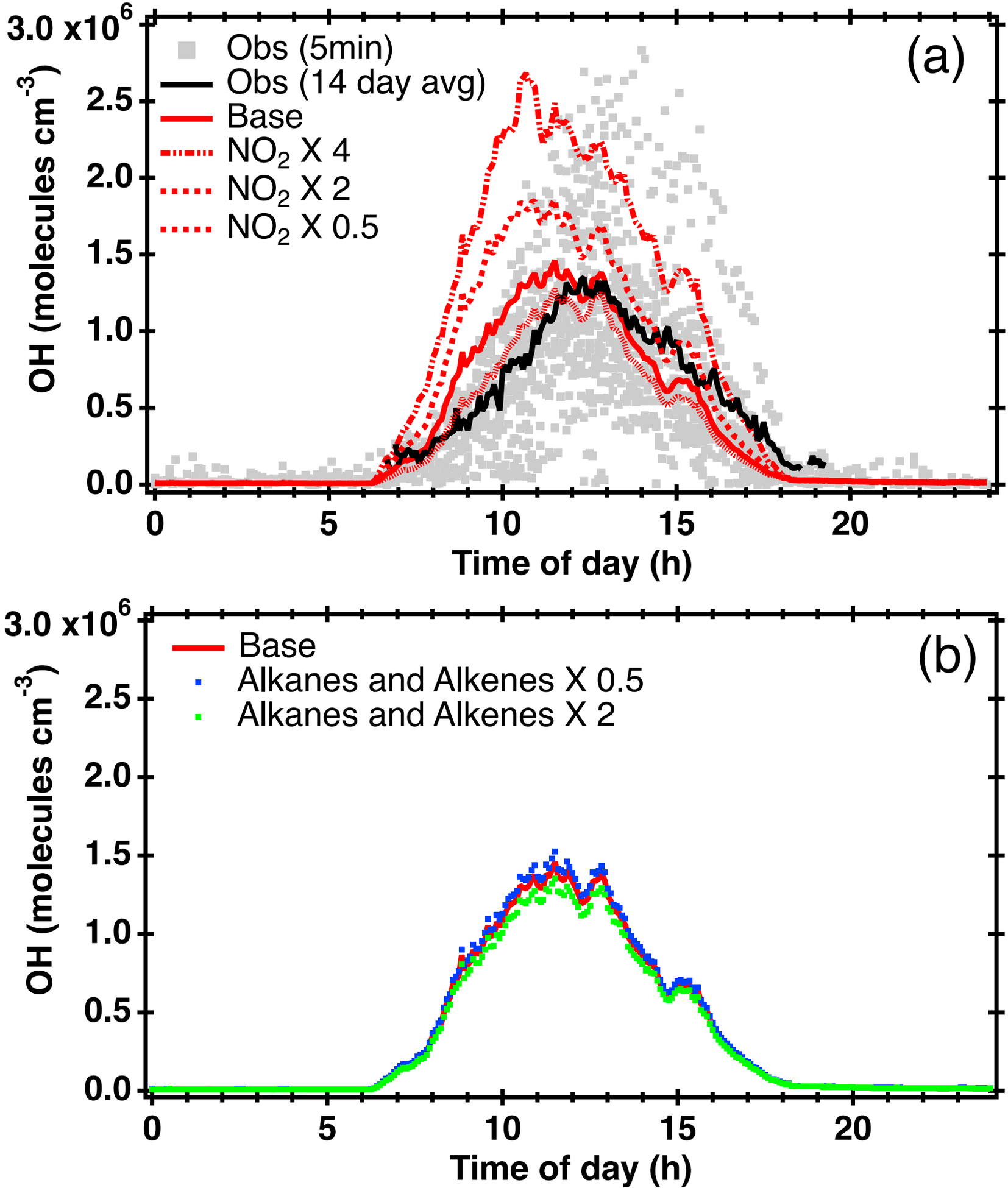
(a)
Obs (5min)
Obs (14 day avg)
Base
NO2 X 4
NO2 X 2
NO2 X 0.5
OH (molecules cm-3)
3.0 x10^6
2.5
2.0
1.5
1.0
0.5
0.0
0
5
10
15
20
Time of day (h)
(b)
Base
Alkanes and Alkenes X 0.5
Alkanes and Alkenes X 2
OH (molecules cm-3)
3.0 x10^6
2.5
2.0
1.5
1.0
0.5
0.0
0
5
10
15
20
Time of day (h)

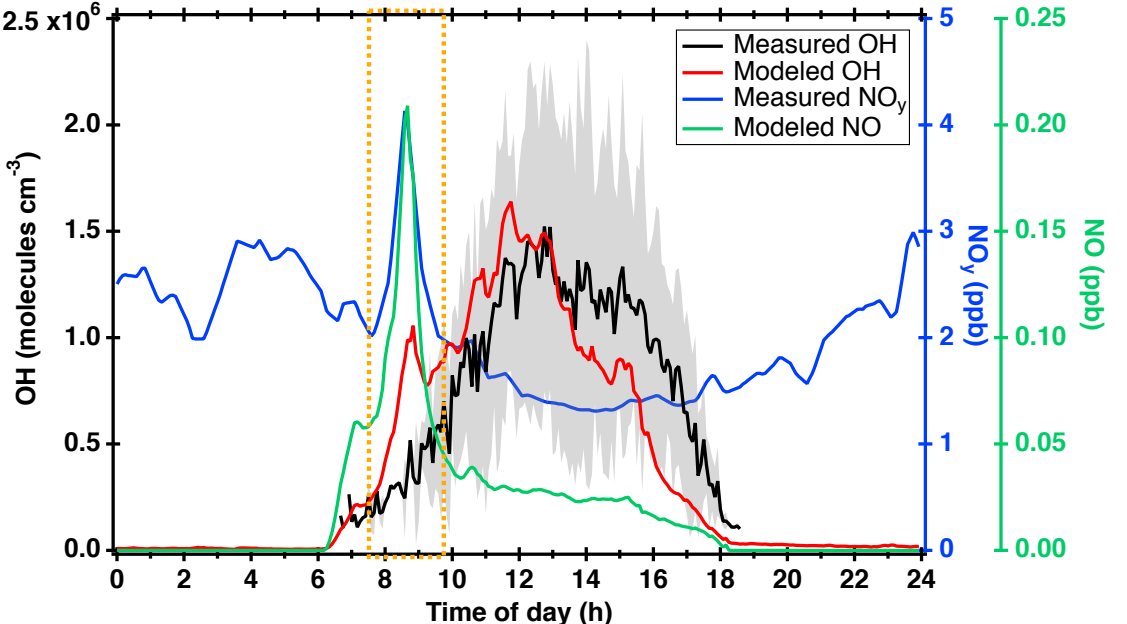
2.5 x10^6
2.0
1.5
1.0
0.5
0.0
OH (molecules cm^-3)
0
2
4
6
8
10
12
14
16
18
20
22
24
Time of day (h)
5
4
3
2
1
0
NO_y (ppb)
0.25
0.20
0.15
0.10
0.05
0.00
NO (ppb)
Measured OH
Modeled OH
Measured NO_y
Modeled NO

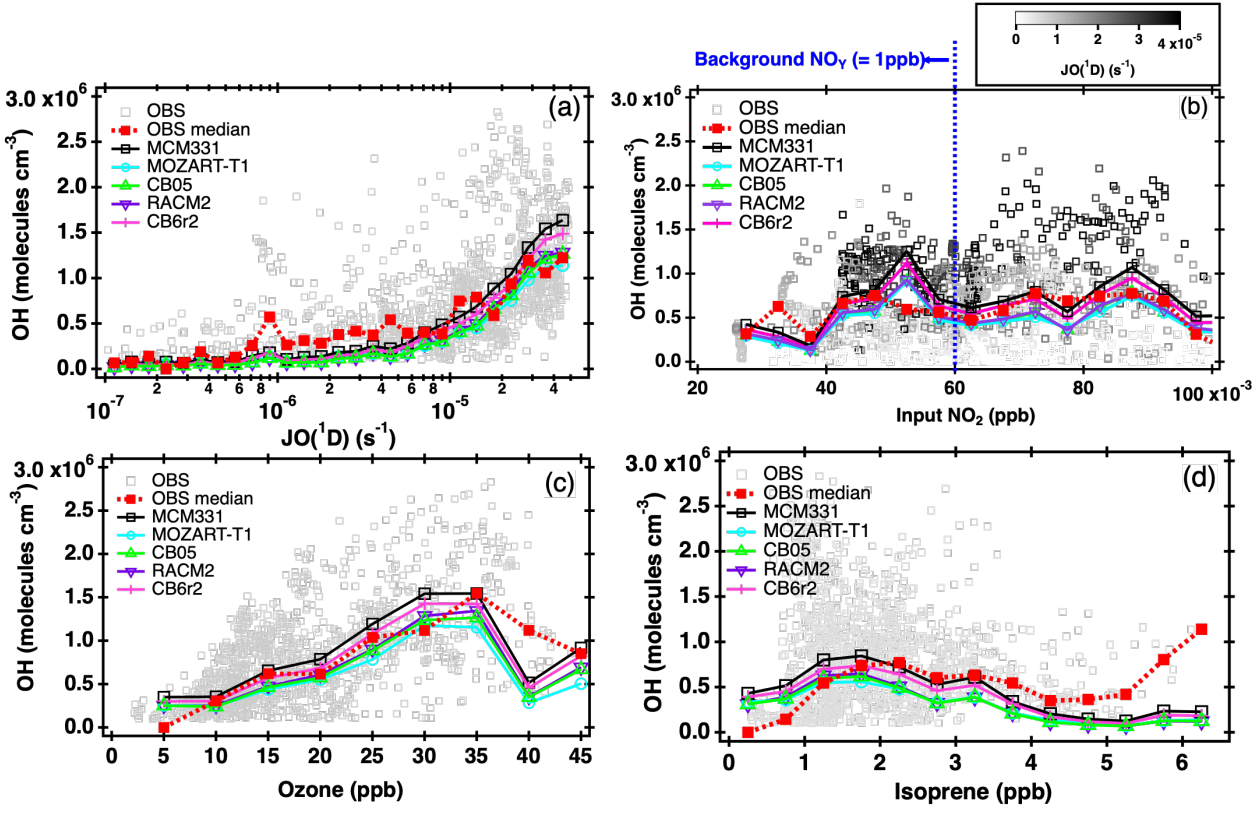
(a)
OBS
OBS median
MCM331
MOZART-T1
CB05
RACM2
CB6r2
OH (molecules cm^{-3})
3.0 x10^6
JO(^{1}D) (s^{-1})
(b)
Background NO$_Y$ (= 1ppb)
0 1 2 3 4 x10^{-5}
JO(^{1}D) (s^{-1})
Input NO$_2$ (ppb)
100 x10^{-3}
(c)
Ozone (ppb)
(d)
Isoprene (ppb)

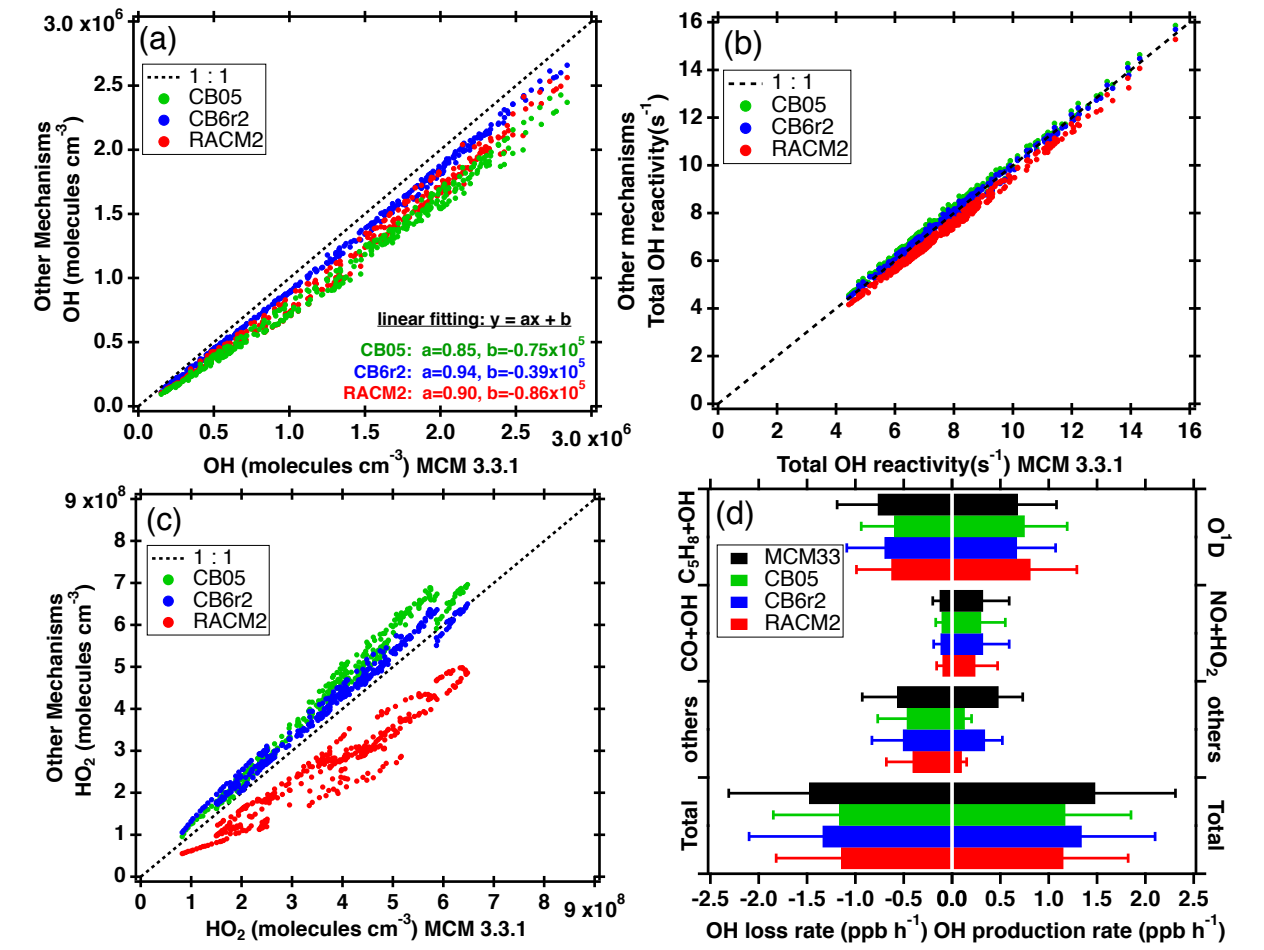
(a)
1 : 1
CB05
CB6r2
RACM2
linear fitting: y = ax + b
CB05: a=0.85, b=-0.75x10^5
CB6r2: a=0.94, b=-0.39x10^5
RACM2: a=0.90, b=-0.86x10^5
Other Mechanisms OH (molecules cm^-3)
OH (molecules cm^-3) MCM 3.3.1
3.0 x10^6
(b)
Other mechanisms Total OH reactivity(s^-1)
Total OH reactivity(s^-1) MCM 3.3.1
(c)
Other Mechanisms HO2 (molecules cm^-3)
HO2 (molecules cm^-3) MCM 3.3.1
9 x10^8
(d)
MCM33
CB05
CB6r2
RACM2
C5H8+OH
CO+OH
others
Total
O1D
NO+HO2
others
Total
OH loss rate (ppb h^-1)
OH production rate (ppb h^-1)